JOURNAL OF COMPUTATIONAL PHYSICS **142,** 370–411 (1998)
ARTICLE NO. CP985931

Accurate Navier–Stokes Investigation of Transitional and Turbulent Flows in a Circular Pipe

V. G. Priymak* and T. Miyazaki†

**Institute for Mathematical Modeling, Russian Academy of Sciences, Miusskaya Square 4-A, Moscow, 125047, Russia; †Department of Mechanical Engineering, Kokushikan University, 4-28-1, Setagaya, Setagaya-ku, Tokyo, 154, Japan*

Received January 9, 1997; revised January 27, 1998

A new, fast, accurate, and roundoff-error robust numerical technique for integrating unsteady incompressible Navier–Stokes equations in cylindrical coordinates is presented. The algorithm is based on a special change of dependent variables which avoids the singularity problem and provides high accuracy and computational efficiency. Accuracy and stability of the method are thoroughly tested for the model problem of transitional and turbulent flows in an infinite circular pipe. Verification of the algorithm includes two issues. First, spectral characteristics of the Hagen–Poiseuille flow stability problem are compared with those of the discrete linearized Navier–Stokes operator. Secondly, the results of direct Navier–Stokes simulation of all stages of laminar-turbulent transition in a circular pipe at Reynolds number of 4000 are presented. Time evolution of finite-amplitude disturbances of laminar flow was calculated until the statistically stationary turbulent flow regime was established. In addition to common statistical analysis, the possibility of turbulence description by means of velocity fields having certain symmetries is examined. Thus, the algorithm presented seems to be a ready-to-use robust tool for accurate investigation and further parametric studies of both transition mechanisms and fully developed turbulent flow regimes.

I. INTRODUCTION

In this paper we concern ourselves with the classical problem of Poiseuille flow stability in an infinite circular pipe $\mathcal{G} = \{\mathbf{r} = (r, \varphi, x) : 0 \le r \le R, 0 \le \varphi < 2\pi, |x| < \infty\}$. More than a century ago O. Reynolds [1] suggested that the instability of stationary pipe flows may be the reason for transition to turbulence and since then numerous attempts were undertaken to verify this hypothesis. Continuing interest in the problem is based on the desire to gain an insight into laminar-turbulent transition phenomena and its control. The pipe Poiseuille flow

0021-9991/98 $25.00

stability problem is of special interest here because it is one of the simplest mathematical idealizations of O. Reynolds experiments.

The main objective of our work is to develop a fast, accurate, and robust Navier–Stokes algorithm suitable for *further parametric studies* of pipe Poiseuille flow stability and related problems. The algorithm constructed covers: (a) direct numerical integration of three-dimensional nonstationary incompressible Navier–Stokes equations in cylindrical geometry with coordinate singularities at supercritical Reynolds numbers; (b) discretization and efficient solution of the eigenvalue problem for the linearized Navier–Stokes operator. Both issues are based on a new change of dependent variables for Navier–Stokes equations in cylindrical coordinates.

The set of key formulas as well as the results of numerical verification at physically meaningful parameters of the problem is presented in the following sections. Algorithm testing includes the investigation of temporal stability of pipe Poiseuille flow both in linear (i.e., with respect to infinitesimal disturbances) and in general nonlinear cases. In particular, we present results of direct Navier–Stokes simulation of laminar-turbulent transition in a circular pipe at a supercritical Reynolds number of 4000. Initial disturbances of laminar flow were specified using nonaxisymmetric eigenfunctions of the Navier–Stokes equations linearized about the parabolic velocity profile. Time evolution of finite-amplitude disturbances was calculated until the statistically stationary turbulent flow regime was established. Thus, the algorithm presented seems to be a ready-to-use tool for accurate investigation of both transition mechanisms and fully developed turbulent flow regimes.

Another new result of this paper is that we have shown analytically and numerically that in contrast to the plane channel and flat plate boundary layer flows the pipe flow turbulence cannot be described by means of Navier–Stokes solutions having certain symmetries (e.g., incorporating the φ-expansion restrictions).

As far as we know this is the first direct simulation of all stages of laminar-turbulent transition in a circular pipe. In some previous Navier–Stokes simulations of pipe turbulence (see, e.g., Priymak [2], Eggels *et al.* [3]) initial conditions were to some extent close to experimental data thus being *a priori* close to the desired result. In computations of Nikitin [4] initial flow field was produced by a random number generator that essentially limits the possibility of physical interpretation and reproduction of the results. Initial stages of laminar-turbulent transition in a pipe were thoroughly examined by O'Sullivan and Breuer [5, 6]. Difficulties associated with the simulation of the late stages are well known to us also. Our former numerical techniques [7, 8] are well suited for the computation of fully developed (statistically steady) turbulent flows as well as of the initial stages of laminar-turbulent transition but demand the repeating filtering of high-frequency modes at the late stages. Notice in addition that Eggels *et al.* [3] and Nikitin [4] utilized finite difference methods to discretize Navier–Stokes equations. The complexity of their finite difference computations seems to be somewhat lower compared to that of our spectral method. On the other hand accuracy of the spectral approach is higher: the details of, e.g., the space-time structure of the turbulent boundary layer may not be accurately described by finite difference methods which suffer from noticeable dispersion and diffusion errors.

Direct Navier–Stokes simulation of all stages of laminar-turbulent transition carried out in the present work seems to be interesting in several aspects. From the hydrodynamic point of view this is one in a few direct theoretical indications of the instability of the fully developed stationary pipe flow with respect to finite amplitude disturbances. In the computational aspect the possibility of calculating the total temporal evolution of initial disturbances by

means of a unique algorithm without its tuning at different stages of transition is extremely attractive, above all, because such a strategy leaves fixed the conditions of the numerical experiment similar to those that take place in the laboratory. The latter facilitates the monitoring of accuracy and reliability of the results obtained. Fixed conditions of simulation are important also for parameter studies of Poiseuille flow stability including investigation of the disturbance structure and amplitude influence on the transition scenario. In addition, the possibility of using a robust algorithm for the simulation of all stages of temporal transition allows one to rely on suitability to use its modifications for more complicated (and more realistic) spatial transition calculations with nonperiodic inflow-outflow boundary conditions.

Until now, most of the analytic and numerical works dealt with the linear stability of pipe Poiseuille flow. Careful investigations demonstrate the stability of a parabolic velocity profile with respect to axisymmetric as well as nonaxisymmetric disturbances at all Reynolds numbers [9]. In the axisymmetric case there also exists the rigorous proof of linear stability [10]. Mathematically, investigation of the stability in the linear approach reduces to the linearization of the Navier–Stokes operator about the parabolic velocity profile, consequent diagonalization, and analysis of eigenvalues. In the present work we are not concerned with numerical methods based on the determination of a few leading eigenvalues defining an asymptotic stability of the stationary solution. On the contrary, we are interested in algorithms able to calculate the full set of eigenvalues of the Navier–Stokes operator for the following reasons.

First, according to modern concepts the local growth of asymptotically stable disturbances can play an important role in triggering transition. At least two mechanisms of such a behaviour are proposed: an algebraic growth of eigenfunctions closely associated with the near degeneracy of eigenvalues [11] and the so-called transient growth stipulated by the nonorthogonality of eigenfunctions of the linear stability operator [12]. In both cases it is suggested to compose an initial disturbance as a superposition of several specially selected eigenfunctions corresponding to eigenvalues from different parts of the spectrum. These eigenfunctions and eigenvalues have to be computed with high accuracy. The question of whether the mechanism indicated can really launch the nonlinear interactions and finally result in the transition to turbulence remains undecided (see, e.g., [5, 6]) and needs further verification.

Second, the knowledge of the complete set of numerical eigenvalues $\{\bar{\lambda}_k\}_{k=1}^{K}$, $re\bar{\lambda}_k \geq re\bar{\lambda}_{k+1}$ where K depends on the resolution is necessary for the discretization quality control. Among the leading values $\bar{\lambda}_k$, $k \simeq 1, 2, \ldots, K/3$ there must be no "spurious" (see also [13]) or other parasitic eigenvalues bearing any relation to the pipe flow spectrum. Eigenvalues $\bar{\lambda}_k$, $k \geq 2K/3$ (the upper third of a numerical spectrum) always correspond to the numerical rubbish and strongly depend on the discretization technique. Nevertheless, the upper edge of the spectrum essentially affects the stability of explicit as well as the convergence and accuracy of implicit time advancing schemes. Thus, the calculation and analysis of the full set of numerical eigenvalues serves as a convenient tool for an *a priori* monitoring of the Navier–Stokes spatial and temporal discretizations.

Numerical solution of the linear stability problem implies the Navier–Stokes spatial discretization followed by the reducing of discrete equations to a standard eigenvalue problem $\lambda\mathbf{x} = A\mathbf{x}$. Eigenvalues λ may then be calculated by means of the QR-algorithm. Certain difficulties arise when accurately approximating Navier–Stokes equations near the coordinate singularity ($r = 0$). Poor discretization may easily lead to low accuracy and sensitivity of the results to the roundoff errors. From cylindrical symmetry of the problem it follows

that the sought for solution may be written as

$$\mathbf{v}(\mathbf{r}, t) = \sum_{n=-\infty}^{\infty} \mathbf{v}_n^F(r, x, t) e^{in\varphi}, \qquad \mathbf{v}_n^{F^*} = \mathbf{v}_{-n}^F, \; i^2 = -1,$$

with an integration domain $\mathcal{G}' = \{0 \le r \le R, |x| < \infty\}$ for the Navier–Stokes equations written in terms of Fourier coefficients $\mathbf{v}_n^F$. Since there is no physical boundary at $r = 0$, certain numerical conditions should be imposed at the polar axis that is now a part of domain $\mathcal{G}'$ boundary. Analytic vector and scalar functions have special behaviour [14] near the singularities that can be exploited when formulating the numerical boundary conditions. Spectral and pseudospectral algorithms developed in [5, 7, 12, 15–19] take into account the stated behaviour of analytic functions thus preserving high accuracy. However, the issue of computational efficiency of the discrete Navier–Stokes solver is developed far less satisfactorily, especially concerning the possibility to exploit fast transforms for the evaluations of nonlinear terms (we can refer here only to Bouaoudia and Marcus [20]).

In the present paper we do not require the Navier–Stokes solutions to meet exactly the behaviour of analytic functions at $r \to 0$. We require the weaker condition that the Navier–Stokes equations and their divergence be nonsingular at the origin. Such Navier–Stokes solutions satisfy the parity relations (i.e., even-odd properties of $\mathbf{v}_n^F$ as functions of r depending on the parity of n) just the same as analytic functions do. If the sought for infinitely differentiable Navier–Stokes solutions prove to be analytic their Fourier coefficients $\mathbf{v}_n^F$ may be extended to the functions on the interval $[-R, R]$. In this case the Chebyshev interpolation polynomials (just even or just odd ones depending on the parity of n) may be used for the approximation of velocity and pressure with spectral accuracy. Note that the above arguments on the point of spectral convergence are not rigorous: we don't know if the turbulent Navier–Stokes solutions are analytic functions or not. Nevertheless, in Section VIII we demonstrate multiple numerical indications of spectral convergence when using the half Chebyshev grid on radial nodes.

In the context of a linear stability problem it is of special interest to devise an algorithm which reduces the discrete equations to the standard eigenvalue problem, is economical, and is somewhat insensitive to roundoff errors. As for the Navier–Stokes time integration we need an economical and fast solver for the nonlinear algebraic system of equations defining the velocity components on a new time level. A new algorithm is based on a special change of dependent variables which avoids the singularity problem and provides high accuracy and computational efficiency. In contrast with our previous approaches [7] we require not only the condition that Navier–Stokes equations (in new variables) should be nonsingular but that their divergence should be nonsingular as well. Spatial discretization is trigonometric approximation in φ and x and Chebyshev collocation in r. The time advancement scheme is Crank–Nicolson for the viscous term, backward Euler for the pressure, and a second-order predictor-corrector type scheme for nonlinear terms. The incompressibility constraint is enforced at the new time level. The Poisson equation for the pressure is obtained from discretized Navier–Stokes equations by means of equivalent matrix operations. The final set of discrete equations can be solved then by means of the influence matrix method with tau correction [21]. As a result, we obtain a numerical method with computational complexity close to that of typical Navier–Stokes algorithms in Cartesian coordinates.

The results presented are really reproducible: the necessary information (including amplitudes and the structure of initial disturbances, parameters of physical and mathematical models, etc.) is given in the following sections.

II. MATHEMATICAL FORMULATION

The stability problem for Poiseuille flow

$$\mathbf{V}^0 = U^0(r)\mathbf{e}_x = -\frac{R^2}{4\nu\rho}\frac{dP_0}{dx}(1 - r^2/R^2)\mathbf{e}_x, \qquad \frac{dP_0}{dx} = \text{const}, \ \mathbf{e}_x = (0, 0, 1), \tag{1}$$

in $\mathcal{G}$ may be set up as the initial boundary-value problem for the Navier–Stokes equations

$$\frac{\partial \mathbf{v}}{\partial t} = -\nabla\Pi + \nu\Delta\mathbf{v} + \mathbf{D}(\mathbf{v}), \tag{2a}$$

$$\nabla \cdot \mathbf{v} = 0, \tag{2b}$$

$$\mathbf{v}|_{r=R} = 0, \qquad \mathbf{v}|_{t=0} = \mathbf{V}^0 + \mathbf{v}_0(\mathbf{r}), \qquad \nabla \cdot \mathbf{v}_0 = 0, \tag{2c}$$

where $\mathbf{v} = v\mathbf{e}_r + w\mathbf{e}_\varphi + u\mathbf{e}_x = (v, w, u)^T$ is the velocity; $\mathbf{D} = (D^v, D^w, D^u)^T = \mathbf{v} \times \boldsymbol{\omega}$; $\boldsymbol{\omega} = (\omega_r, \omega_\varphi, \omega_x)^T = \nabla \times \mathbf{v}$ is the vorticity; Π is the total pressure; ρ and ν are the constant density and kinematic viscosity; and $\mathbf{v}_0 \not\equiv 0$ is a certain initial disturbance of Poiseuille flow.

Since the flow is homogeneous in the x-direction, Eqs. (2) are supplemented with the boundary conditions

$$\mathbf{v}(\mathbf{r}, t) = \mathbf{v}(r, \varphi, x + X, t), \tag{3a}$$

$$\Pi = p_x(t)x + p(\mathbf{r}, t), \qquad p(\mathbf{r}, t) = p(r, \varphi, x + X, t), \tag{3b}$$

$$\bar{U}(t) \stackrel{\text{def}}{=} \frac{1}{\pi R^2}\int_0^R r\,dr\int_0^{2\pi} d\varphi u(\mathbf{r}, t) = \frac{2}{R^2}\int_0^R U^0 r\,dr. \tag{3c}$$

Here the streamwise period X is the parameter of the mathematical model, $p_x(t)$ has the meaning of a space averaged pressure gradient, and Eq. (3c) is the condition of volume flux (mean velocity $\bar{U}$) constancy.

III. BEHAVIOUR OF ANALYTIC FUNCTIONS NEAR THE SINGULARITY

For the formulation of numerical boundary conditions at the polar axis we shall exploit the well known (see, e.g., [14, 16, 17]) asymptotic behaviour of analytic functions at $r \to 0$. To make the article self-contained we include the following theorem.

THEOREM 1. *Suppose that vector* $\mathbf{v}(x, y) = v_x\mathbf{e}_x + v_y\mathbf{e}_y$, $\mathbf{e}_x = (1, 0)$, $\mathbf{e}_y = (0, 1)$, *and scalar* $p(x, y)$ *functions of Cartesian coordinates are analytic for* $(x^2 + y^2)^{1/2} < \epsilon$ (*some* $\epsilon > 0$). *Then, as functions of polar coordinates,* $\mathbf{v}(r, \varphi) = v\mathbf{e}_r + w\mathbf{e}_\varphi$, $f(r, \varphi) = v + iw$, $g(r, \varphi) = v - iw$, *and* $p(r, \varphi)$ *satisfy the relations* $(0 \le r < \epsilon)$

$$q(r, \varphi) = \sum_{n=-\infty}^{\infty} q_n(r)\exp(in\varphi), \qquad q = (f, g, p)^T, \tag{4}$$

$$f_n = r^{|n+1|}\hat{f}_n(r), \qquad g_n = r^{|n-1|}\hat{g}_n(r), \qquad p_n = r^{|n|}\hat{p}_n(r), \tag{5}$$

where

$$\hat{q}_n(r) = \sum_{k=0}^{\infty}\hat{q}_{nk}r^{2k}, \qquad \hat{q} = (\hat{f}, \hat{g}, \hat{p})^T.$$

Notice that these statements can be derived solely from the analysis of Taylor expansions of analytic vector and scalar functions in the vicinity of the polar axis.

COROLLARY 1. *Suppose that the hypotheses of Theorem 1 are satisfied. Then radial* $v(r, \varphi)$ *and azimuth* $w(r, \varphi)$ *components of the vector* $\mathbf{v}$ *must satisfy*

$$q(r, \varphi) = \sum_{n=-\infty}^{\infty} q_n(r) \exp(in\varphi), \qquad q = (v, w)^T, \tag{6}$$

$$q_0 = r\hat{q}_0(r), \qquad q_n = r^{|n|-1}\hat{q}_n(r) \ (n \neq 0), \qquad \hat{q}_n = \sum_{k=0}^{\infty} \hat{q}_{nk} r^{2k}. \tag{7}$$

COROLLARY 2. *Suppose that vector* $\mathbf{v}(r, \varphi, x) = v\mathbf{e}_r + w\mathbf{e}_\varphi + u\mathbf{e}_x$ *and scalar* $p(r, \varphi, x)$ *functions of cylindrical coordinates are periodic in* x *with period* X *and are analytic for* $0 \le r \le \epsilon$ *(some* $\epsilon > 0$*). Then for* $0 \le r \le \epsilon$ *functions* $v, w, u, f = v + iw, g = v - iw, p$ *satisfy*

$$q(r, \varphi, x) = \sum_{n=-\infty}^{\infty} \sum_{m=-\infty}^{\infty} q_{nm}(r) \exp(i2\pi mx/X + in\varphi), \qquad q = (f, g, p, v, w, u)^T, \tag{8}$$

$$\begin{gathered} f_{nm} = r^{|n+1|}\hat{f}_{nm}(r), \qquad g_{nm} = r^{|n-1|}\hat{g}_{nm}(r), \\ (p_{nm}, u_{nm}) = r^{|n|}(\hat{p}_{nm}(r), \hat{u}_{nm}(r)), \\ (v_{nm}, w_{nm}) = r^{|n|-1}(\hat{v}_{nm}(r), \hat{w}_{nm}(r)), \qquad n \neq 0, \\ (v_{0m}, w_{0m}) = r(\hat{v}_{0m}(r), \hat{w}_{0m}(r)), \end{gathered} \tag{9}$$

where

$$\hat{q}_{nm} = \sum_{k=0}^{\infty} \hat{q}_{nmk} r^{2k}, \qquad \hat{q} = (\hat{f}, \hat{g}, \hat{p}, \hat{v}, \hat{w}, \hat{u})^T.$$

IV. NEW DEPENDENT VARIABLES

Approximate solutions of Eqs. (2), (3) we represent by the truncated Fourier series

$$\mathbf{v} = \sum_{n=-N}^{N} \sum_{m=-M}^{M} \mathbf{v}^F_{nm}(r, t) \exp(i\alpha_m x + in\varphi) = \sum_{n=0}^{N} \sum_{m=0}^{M} \mathbf{v}_{nm}(r, \varphi, x, t), \tag{10}$$

$$\left(\mathbf{v}^F_{nm}\right)^* = \mathbf{v}^F_{-n,-m}, \qquad i^2 = -1, \qquad \alpha_m = 2\pi m/X,$$

with an analogous representation for $p(\mathbf{r}, t)$.

Next, we conduct two sequential changes of dependent variables. The first one

$$f_{nm}(r, \varphi, x, t) = v_{nm} + \frac{1}{n}\frac{\partial w_{nm}}{\partial \varphi}, \qquad g_{nm} = v_{nm} - \frac{1}{n}\frac{\partial w_{nm}}{\partial \varphi}, \ n > 0, \tag{11}$$

is well known [14] and widely used to diagonalize vector Laplacian.

The second is a new one

$$
\begin{aligned}
(\tilde{u}_{nm}, \tilde{p}_{nm}) &= r^{-\sigma_n}(u_{nm}, p_{nm}) \qquad (n \geq 0),\\
(\tilde{v}_{0m}, \tilde{w}_{0m}) &= r^{-1}(v_{0m}, w_{0m}),\\
\tilde{f}_{nm} &= r^{-(\sigma_n+1)} f_{nm} \qquad (n > 0),\\
\tilde{g}_{1m} = g_{1m}, &\qquad \tilde{g}_{nm} = r^{-(\sigma_n+1)} g_{nm}\ (n > 1),
\end{aligned}
\tag{12}
$$

where $\sigma_{2k} = 0$ and $\sigma_{2k+1} = 1$ for $k = 0, 1, \ldots$.

Going over to new variables in Eqs. (2) we obtain for certain Fourier mode with n, $m \geq 0$,

$$
\frac{\partial \mathbf{q}_{nm}}{\partial t} = -\nabla \tilde{p}_{nm} + \nu \Delta \mathbf{q}_{nm} + \mathbf{d}_{nm}(\mathbf{q}), \tag{13a}
$$

$$
\nabla \cdot \mathbf{q}_{nm} = 0, \qquad \mathbf{q}_{nm} = \begin{cases} (\tilde{f}_{nm}, \tilde{g}_{nm}, \tilde{u}_{nm})^T, & n > 0 \\ (\tilde{v}_{0m}, \tilde{w}_{0m}, \tilde{u}_{0m})^T, & n = 0, \end{cases} \tag{13b}
$$

$$
\mathbf{q}_{nm}|_{r=R} = 0\ (n \geq 0), \qquad \int_0^R \tilde{u}_{00}(r,t) r\, dr = \int_0^R U^0 r\, dr, \tag{13c}
$$

$$
\tilde{f}_{nm}|_{r=0} = \tilde{u}_{nm}|_{r=0} = \tilde{p}_{nm}|_{r=0} = 0\ (n > 1), \qquad \tilde{g}_{nm}|_{r=0} = 0\ (n > 3). \tag{13d}
$$

Here for $n = 0$,

$$
\begin{aligned}
\nabla \tilde{p}_{0m} &= \left(\frac{1}{r}\frac{\partial}{\partial r}\tilde{p}_{0m}, 0, \frac{\partial}{\partial x}\tilde{p}_{0m} + p_x(t)\delta_{m0} \right)^T,\\
\nabla \cdot \mathbf{q}_{0m} &= \left(r\frac{\partial}{\partial r} + 2 \right)\tilde{v}_{0m} + \frac{\partial}{\partial x}\tilde{u}_{0m},\\
\Delta \mathbf{q}_{0m} &= \begin{pmatrix} \left(\frac{\partial^2}{\partial r^2} + \frac{3}{r}\frac{\partial}{\partial r} - \alpha_m^2\right)\tilde{v}_{0m} \\ \left(\frac{\partial^2}{\partial r^2} + \frac{3}{r}\frac{\partial}{\partial r} - \alpha_m^2\right)\tilde{w}_{0m} \\ \nabla^2 \tilde{u}_{0m} \end{pmatrix};
\end{aligned}
\tag{14a}
$$

for $n = 1$,

$$
\begin{aligned}
\nabla \tilde{p}_{1m} &= \left(\frac{1}{r}\frac{\partial}{\partial r}\tilde{p}_{1m}, \left(r\frac{\partial}{\partial r} + 2 \right)\tilde{p}_{1m}, \frac{\partial}{\partial x}\tilde{p}_{1m} \right)^T,\\
\nabla \cdot \mathbf{q}_{1m} &= \left(r\frac{\partial}{\partial r} + 4 \right)\tilde{f}_{1m} + \frac{1}{r}\frac{\partial}{\partial r}\tilde{g}_{1m} + 2\frac{\partial}{\partial x}\tilde{u}_{1m},\\
\Delta \mathbf{q}_{1m} &= \begin{pmatrix} \left(\frac{\partial^2}{\partial r^2} + \frac{5}{r}\frac{\partial}{\partial r} - \alpha_m^2\right)\tilde{f}_{1m} \\ \left(\frac{\partial^2}{\partial r^2} + \frac{1}{r}\frac{\partial}{\partial r} - \alpha_m^2\right)\tilde{g}_{1m} \\ \nabla^2 \tilde{u}_{1m} \end{pmatrix};
\end{aligned}
\tag{14b}
$$

for $n > 1$,

$$\nabla\tilde{p}_{nm} = \left(\left(\frac{1}{r}\frac{\partial}{\partial r} - \frac{(n-\sigma_n)}{r^2}\right)\tilde{p}_{nm}, \left(\frac{1}{r}\frac{\partial}{\partial r} + \frac{(n+\sigma_n)}{r^2}\right)\tilde{p}_{nm}, \frac{\partial}{\partial x}\tilde{p}_{nm}\right)^T,$$

$$\nabla\cdot\mathbf{q}_{nm} = \left(r\frac{\partial}{\partial r} + (n+\sigma_n+2)\right)\tilde{f}_{nm} + \left(r\frac{\partial}{\partial r} - (n-\sigma_n-2)\right)\tilde{g}_{nm} + 2\frac{\partial}{\partial x}\tilde{u}_{nm}, \quad (14c)$$

$$\Delta\mathbf{q}_{nm} = \begin{pmatrix} \left(\frac{\partial^2}{\partial r^2} + \frac{2\sigma_n+3}{r}\frac{\partial}{\partial r} - \frac{(n+1)^2-(\sigma_n+1)^2}{r^2} - \alpha_m^2\right)\tilde{f}_{nm} \\ \left(\frac{\partial^2}{\partial r^2} + \frac{2\sigma_n+3}{r}\frac{\partial}{\partial r} - \frac{(n-1)^2-(\sigma_n+1)^2}{r^2} - \alpha_m^2\right)\tilde{g}_{nm} \\ \nabla^2\tilde{u}_{nm} \end{pmatrix},$$

and

$$\nabla^2\tilde{u}_{nm} = \left(\frac{\partial^2}{\partial r^2} + \frac{2\sigma_n+1}{r}\frac{\partial}{\partial r} - \frac{\left(n^2-\sigma_n^2\right)}{r^2} - \alpha_m^2\right)\tilde{u}_{nm}$$

for arbitrary $n \geq 0$. Note also, that axis conditions (13d) immediately follow from Corollary 2.

As for the Fourier coefficients of nonlinearity we obtain

$$\mathbf{d}_{nm} = \left(d^f_{nm}, d^g_{nm}, d^u_{nm}\right)^T, \qquad d^u_{nm} = r^{-\sigma_n} D^u_{nm}\ (n \geq 0),$$

$$d^f_{nm} = \begin{cases} r^{-1}D^v_{0m}, & n = 0 \\ r^{-(\sigma_n+1)}\left(D^v_{nm} + \frac{1}{n}\frac{\partial}{\partial\varphi}D^w_{nm}\right), & n > 0, \end{cases}$$

$$d^g_{nm} = \begin{cases} r^{-1}D^w_{0m}, & n = 0 \\ \left(D^v_{1m} - \frac{\partial}{\partial\varphi}D^w_{1m}\right), & n = 1 \\ r^{-(\sigma_n+1)}\left(D^v_{nm} - \frac{1}{n}\frac{\partial}{\partial\varphi}D^w_{nm}\right), & n > 1. \end{cases} \quad (15)$$

Notice that in spite of the fact that Eqs. (13)–(14) do contain negative powers of r, they may be treated as nonsingular. This statement follows directly from Corollary 2 (new variables may be represented as a series of even powers of r in the vicinity of $r = 0$), an explicit form of $\nabla\tilde{p}_{nm}$, $\Delta\mathbf{q}_{nm}$, $\nabla\cdot\mathbf{q}_{nm}$, and axis conditions (13d). And what is more, not only Navier–Stokes equations (13) are nonsingular but their divergence is nonsingular as well. The latter turns out to be very important for the derivation of special matrix identities—the foundation of an efficient discrete Navier–Stokes solver (see Section V). We stress in addition that because of the asymptotic behaviour of the nonlinear terms $D^{v,w,u}_{nm}$, Eqs. (15) also do not contain singularities. This asymptotics is the basis of a fast and accurate algorithm for the calculation of Navier–Stokes nonlinear terms and is analysed in Section VI.

V. DISCRETE NAVIER–STOKES EQUATIONS

To integrate numerically Navier–Stokes equations (13) we exploit the so-called method of lines separating the time and spatial discretizations.

A. *Time Stepping*

Temporal discretization is carried out by means of the implicit second-order scheme

$$\begin{gathered}\frac{\mathbf{q}_{nm}^{k+1}-\mathbf{q}_{nm}^{k}}{\Delta t}=-\nabla\tilde{p}_{nm}^{k+1}+\nu\Delta\left(\frac{\mathbf{q}_{nm}^{k+1}+\mathbf{q}_{nm}^{k}}{2}\right)+\mathbf{d}_{nm}\left(\frac{\mathbf{q}^{k+1}+\mathbf{q}^{k}}{2}\right),\\ \nabla\cdot\mathbf{q}_{nm}^{k+1}=0,\\ \mathbf{q}_{nm}^{k+1}\big|_{r=R}=0\ (n\geq 0),\qquad \int_0^R\tilde{u}_{00}^{k+1}r\,dr=\int_0^R U^0 r\,dr,\\ \tilde{f}_{nm}^{k+1}\big|_{r=0}=\tilde{u}_{nm}^{k+1}\big|_{r=0}=\tilde{p}_{nm}^{k+1}\big|_{r=0}=0\ (n>1),\qquad \tilde{g}_{nm}^{k+1}\big|_{r=0}=0\ (n>3),\end{gathered}\tag{16}$$

where $\mathbf{q}_{nm}^{k}=\mathbf{q}_{nm}(r,\varphi,x,t_k)$, $\tilde{p}_{nm}^{k}=\tilde{p}_{nm}(r,\varphi,x,t_k)$, and $\Delta t=t_{k+1}-t_k$ is a time step. That is, we assume the use of a Crank–Nicolson scheme for viscous terms, backward Euler for the pressure, and a certain second order scheme for nonlinear term $\mathbf{d}$. Note that if you use e.g., a Crank–Nicolson scheme for the pressure and introduce then a new variable $\tilde{p}_{nm}^{k+1}=(\tilde{p}_{nm}^{k+1}+\tilde{p}_{nm}^{k})/2$ you will obtain just the same scheme as in the case of backward Euler. In fact, the pressure term is eliminated then from Eqs. (16) (see Section V (D)).

To solve Eqs. (16) the following successive approximations method is utilized,

$$\left(\frac{2}{\Delta t}-\nu\Delta\right)\overset{(s)}{\mathbf{q}}{}_{nm}^{k+1}+2\nabla\overset{(s)}{\tilde{p}}{}_{nm}^{k+1}=\mathbf{a}_{nm},\tag{17a}$$

$$\nabla\cdot\overset{(s)}{\mathbf{q}}{}_{nm}^{k+1}=0,\tag{17b}$$

$$\overset{(s)}{\mathbf{q}}{}_{nm}^{k+1}\big|_{r=R}=0\ (n\geq 0),\qquad \int_0^R\overset{(s)}{\tilde{u}}{}_{00}^{k+1}r\,dr=\int_0^R U^0 r\,dr,\tag{17c}$$

$$\overset{(s)}{\tilde{f}}{}_{nm}^{k+1}\big|_{r=0}=\overset{(s)}{\tilde{u}}{}_{nm}^{k+1}\big|_{r=0}=\overset{(s)}{\tilde{p}}{}_{nm}^{k+1}\big|_{r=0}=0\ (n>1),\qquad \overset{(s)}{\tilde{g}}{}_{nm}^{k+1}\big|_{r=0}=0\ (n>3),\tag{17d}$$

where $s=1,2,\ldots,S$ is the iteration counter. Here the right-hand side of Eq. (17a) is a known value being the function of velocity components relating to time level t_k and preceding iterative loop:

$$\mathbf{a}_{nm}=\left(\frac{2}{\Delta t}+\nu\Delta\right)\mathbf{q}_{nm}^{k}+2\mathbf{d}_{nm}\left(\frac{\overset{(s-1)}{\mathbf{q}}{}^{k+1}+\mathbf{q}^{k}}{2}\right).$$

If we calculate initial approximation by the formulas

$$\overset{(0)}{\mathbf{q}}{}_{nm}^{k+1}=2\mathbf{q}_{nm}^{k}-\mathbf{q}_{nm}^{k-1},$$

then Eqs. (17) define the time integration scheme of $O(\Delta t^2)$ approximation order for arbitrary $S\geq 1$. For all the computer runs described in Section VIII(C) we utilized $S=2$ thus carrying out calculations by means of a certain explicit scheme of predictor-corrector type. Exhaustive *a priori* analysis of scheme (17) accuracy and stability may be conducted by examining the eigenvalues spectrum of the linearized discrete Navier–Stokes equations (see Section VIII(B)).

B. *Interpolation Polynomials and Collocation Method*

New variables $\mathbf{q}_{nm}$ as functions of r we approximate by polynomials

$$\mathbf{q}_{nm}(r,\varphi,x,t)=\sum_{j=0}^{Q}\mathbf{q}_{nmj}(\varphi,x,t)h_j(r),\qquad \mathbf{q}_{nmj}=\mathbf{q}_{nm}|_{r=r_j},$$

$$h_j=(2\varrho_j/Q)\sum_{l=0}^{Q}\varrho_l T_{2l}(r_j/R)T_{2l}(r/R),\qquad j=0,1,\ldots,Q \tag{18}$$

$$r_j=R\cos\frac{\pi j}{2Q},\qquad \varrho_0=\varrho_Q=1/2,\qquad \varrho_l=1\ (l\neq 0,Q).$$

Here T_{2l} are Chebyshev polynomials of the first kind. It should be stressed that only even Chebyshev polynomials are used in the expansion (18) and r_j varies from 0 for $j=Q$ to R for $j=0$, so that at the origin there is no clustering of collocation points in r. The possibility of representation (18) follows immediately from Corollary 2 and formulas (12). Notice also that spectral representations (18) do not meet exactly pole conditions typical for analytic functions. We require the weaker conditions (13d) to be satisfied. If the sought for infinitely differentiable Navier–Stokes solutions turn out to be analytic they may be smoothly extended to the functions on the interval $[-R, R]$ thus providing spectral convergence when using a half Chebyshev grid on radial nodes.

We continue by defining the $(Q+1)\times(Q+1)$ matrices

$$C_{lj}=\left.\frac{d^2h_j}{dr^2}\right|_{r=r_l},\qquad B_{lj}=\left.\frac{1}{r}\frac{dh_j}{dr}\right|_{r=r_l},$$
$$D_{lj}=\left.r\frac{dh_j}{dr}\right|_{r=r_l},\qquad S_{lj}=\left.\frac{h_j(r)-h_j(0)}{r^2}\right|_{r=r_l}, \tag{19}$$
$$\mathbf{E}_{lj}=\delta_{lj},\qquad l,j=0,1,\ldots,Q$$

being the finite-dimensional analogues of the corresponding differential operators from Eqs. (14). So, for example, we use the following approximation for the values of the second derivative,

$$\left.\frac{\partial^2\mathbf{q}_{nm}}{\partial r^2}\right|_{r=r_l}=\sum_{j=0}^{Q}C_{lj}\mathbf{q}_{nmj},\qquad l=0,1,\ldots,Q,$$

and similar formulas for $(1/r)\partial\mathbf{q}_{nm}/\partial r|_{r=r_l}$ and $r\,\partial\mathbf{q}_{nm}/\partial r|_{r=r_l}$.

As to the operator $1/r^2$, we obtain with regard to axis conditions (13d)

$$\frac{1}{r^2}\tilde{g}_{nm}|_{r=r_l}=\sum_{j=0}^{Q}S_{lj}\tilde{g}_{nmj},\qquad l=0,1,\ldots,Q, \tag{20}$$

for arbitrary $n>3$. Since an equality $\tilde{g}_{nm}/r^2=(\tilde{g}_{nm}-\tilde{g}_{nm}|_{r=0})/r^2$ is correct for $n>3$, formulas (20) may be used to approximate expressions $[(n-1)^2-(\sigma_n+1)^2](1/r^2)\tilde{g}_{nm}$ in Eqs. (14c) for arbitrary $n>1$. The reason is that for $n=2,3$ (when $\tilde{g}_{nm}|_{r=0}\not\equiv 0$) an expression in square brackets becomes zero. Formulas (20) may also be used to approximate expressions $(1/r^2)\tilde{f}_{nm}$, $(1/r^2)\tilde{u}_{nm}$, and $(1/r^2)\tilde{p}_{nm}$ in Eqs. (14c) when $n>1$.

In spite of the fact that Eqs. (19) do contain negative powers of r, computations may be conducted without any loss of accuracy provided that recurrence relations for Chebyshev

polynomials (see, e.g., [22]) are exploited. The resultant computational formulas for matrix elements we present in Appendix A.

For the discretization of Eqs. (17) in r we make use of the pseudospectral technique with collocation nodes r_j defined in(18). Finally, we obtain the following set of semi-discrete equations (the case $\alpha_m, n > 0$):

$$\left(\frac{2}{\Delta t}E - \nu L^f\right)\mathbf{F}|_l + R^f\mathbf{P}|_l = \tau_0^f\delta_{l0} + \tau_Q^f(1-\delta_{n1})\delta_{lQ} + a_l^f, \quad l = 0, 1, \ldots, Q, \qquad F_0 = 0, \qquad F_Q = 0\ (n > 1) \tag{21a}$$

$$\left(\frac{2}{\Delta t}E - \nu L^g\right)\mathbf{G}|_l + R^g\mathbf{P}|_l = \tau_0^g\delta_{l0} + r_Q^g(1-\delta_{n1}-\delta_{n2}-\delta_{n3})\delta_{lQ} + a_l^g, \quad l = 0, 1, \ldots, Q, \qquad G_0 = 0, \qquad G_Q = 0\ (n > 3) \tag{21b}$$

$$\left(\frac{2}{\Delta t}E - \nu L^u\right)\mathbf{U}|_l + \frac{\partial}{\partial x}P_l = \tau_0^u\delta_{l0} + \tau_Q^u(1-\delta_{n1})\delta_{lQ} + a_l^u, \quad l = 0, 1, \ldots, Q, \qquad U_0 = 0, \qquad U_Q = 0\ (n > 1) \tag{21c}$$

$$H^f\mathbf{F}|_l + H^g\mathbf{G}|_l + 2\frac{\partial}{\partial x}U_l = 0, \qquad l = \begin{cases} 0, 1, \ldots, Q, & n = 1 \\ 0, 1, \ldots, Q-1, & n > 1, \end{cases} \quad P_Q = 0 \qquad (n > 1). \tag{21d}$$

Here $\tau_l^f, \tau_l^g, \tau_l^u (l = 0, Q)$ are the so-called tau terms [23] having the meaning of equations residual at the boundaries of domain $\mathcal{G}$; δ_{lj} is the Kronecker delta; $\mathbf{P} \stackrel{\text{def}}{=} (P_0, P_1, \ldots, P_Q)^T$, $P_j(\varphi, x) = 2\overset{(s)}{\tilde{p}}{}^{k+1}_{nmj} = 2\overset{(s)}{\tilde{p}}{}^{k+1}_{nm}|_{r=r_j}$; $\mathbf{F} \stackrel{\text{def}}{=} (F_0, F_1, \ldots, F_Q)^T$, $F_j(\varphi, x) = \overset{(s)}{\tilde{f}}{}^{k+1}_{nmj}$, analogously for $\mathbf{G}$ and $\mathbf{U}$. Terms a_l^f, a_l^g, and a_l^u include the discretization of nonlinear terms and are known values at a new time level:

$$a_l^f = \left(\frac{2}{\Delta t}E + \nu L^f\right)\mathbf{F}^k|_l + 2d^f_{nml}\left(\frac{\overset{(s-1)}{\mathbf{q}}{}^{k+1} + \mathbf{q}^k}{2}\right), \quad \mathbf{F}^k \stackrel{\text{def}}{=} \left(F_0^k, F_1^k, \ldots, F_Q^k\right)^T, \qquad F_j^k = \tilde{f}^k_{nmj}; \qquad d^f_{nml} = d^f_{nm}\big|_{r=r_l}, \tag{22}$$

and similarly for a_l^g, a_l^u. Equations analogous to (21) and corresponding to $n = 0$ and $\alpha_m = 0$ we present in Appendix B.

In the case $n > 0$, $(Q+1)\times(Q+1)$ matrices $L^f, L^g, L^u, R^f, R^g, H^f$, and H^g are defined by formulas

$$\begin{pmatrix} L^f \\ L^u \end{pmatrix} = C + \begin{pmatrix} 2\sigma_n + 3 \\ 2\sigma_n + 1 \end{pmatrix} B - \begin{pmatrix} (n+1)^2 - (\sigma_n+1)^2 \\ n^2 - \sigma_n^2 \end{pmatrix} S - \alpha_m^2 E,$$

$$L^g = \begin{cases} C + B - \alpha_m^2 E, & n = 1 \\ C + (2\sigma_n + 3)B - ((n-1)^2 - (\sigma_n+1)^2)S - \alpha_m^2 E, & n > 1, \end{cases} \tag{23}$$

$$R^g = \begin{cases} D + 2E, & n = 1 \\ B + (\sigma_n + n)S, & n > 1, \end{cases} \qquad H^g = \begin{cases} B, & n = 1 \\ D + (\sigma_n - n + 2)E, & n > 1, \end{cases}$$

$$R^f = B + (\sigma_n - n)S, \qquad H^f = D + (\sigma_n + n + 2)E.$$

Grid functions $\mathbf{F}$, $\mathbf{G}$, $\mathbf{U}$, and $\mathbf{P}$ are strongly coupled in Eqs. (21). The latter makes it somewhat difficult to suggest a fast and economical method of solution. On the other hand, suppose there exists an efficient solver for Eqs. (21a)–(21c) provided that $\mathbf{P}$ are known values. In that case it is desirable to reduce Eqs. (21) to the form that allows us to evaluate first $\mathbf{P}$ irrespective of $\mathbf{F}$, $\mathbf{G}$, and $\mathbf{U}$. The possibility of such a solution procedure for Eqs. (21) is considered in the following two subsections and in Section VII.

C. *Special Matrix Identities*

Easily verifiable differential identities

$$\nabla \cdot \Delta \mathbf{q}_{nm} \equiv \nabla^2(\nabla \cdot \mathbf{q}_{nm}), \qquad \nabla \cdot \nabla \tilde{p}_{nm} \equiv \nabla^2 \tilde{p}_{nm}, \ n, m \geq 0,$$

have in case $n > 0$ the following semi-discrete analogues

$$H^f L^f \mathbf{F} + H^g L^g \mathbf{G} + 2\frac{\partial}{\partial x} L^u \mathbf{U} = L^u \left(H^f \mathbf{F} + H^g \mathbf{G} + 2\frac{\partial}{\partial x} \mathbf{U} \right), \tag{24a}$$

$$\frac{1}{2}\left(H^f R^f + H^g R^g - 2\alpha_m^2 E\right)\mathbf{P} = L^u \mathbf{P}. \tag{24b}$$

Again, the case $n = 0$ is considered separately in Appendix B. Formulas (24) follow from

THEOREM 2. *Suppose that differential operators*

$$C = \frac{d^2}{dr^2}, \qquad B = \frac{1}{r}\frac{d}{dr}, \qquad D = r\frac{d}{dr}$$

and operator S

$$Sh = \frac{1}{r^2}(h(r) - h(0))$$

are defined on interpolation polynomials

$$h_j(r) = (2\varrho_j/Q) \sum_{l=0}^{Q} \varrho_l T_{2l}(r_j) T_{2l}(r), \qquad j = 0, 1, \ldots, Q,$$

$$r_j = \cos \pi j/2Q, \qquad \varrho_0 = \varrho_Q = 1/2, \qquad \varrho_l = 1 \ (l \neq 0, Q).$$

Assume that (XY) *is one of the following ordered operator couples:*

$$(CB), (BC), (CD), (DC), (CS), (BD), (DB),$$

$$(BS), (DS), (SD), (CC), (DD), (BB).$$

The matrix identity

$$T^d = X^d Y^d$$

then holds in the case of matrices X^d, Y^d, *and* T^d *with elements*

$$X^d_{lj} = Xh_j|_{r=r_l}, \qquad Y^d_{lj} = Yh_j|_{r=r_l}, \qquad (T^d)_{lj} = XYh_j|_{r=r_l}.$$

Proof. It can be easily shown (see, e.g., [22]) that the result of operation with C, B, D, or S on polynomials $T_{2q}(r)$, $q = 0, 1, \ldots, Q$ may be represented by a (truncated) series of Chebyshev polynomials of degree not higher than $2q$. Denoting with $\tilde{X}^d$, $\tilde{Y}^d$ the matrices of expansion coefficients, we obtain then

$$X^d_{lp} = Xh_p|_{r=r_l} = \frac{2\varrho_p}{Q}\sum_{q'=0}^{Q}\varrho_{q'}T_{2q'}(r_p)XT_{2q'}(r)|_{r=r_l}$$

$$= \frac{2\varrho_p}{Q}\sum_{q'=0}^{Q}\varrho_{q'}T_{2q'}(r_p)\sum_{n=0}^{q'}\tilde{X}^d_{q'n}T_{2n}(r_l), \tag{25a}$$

$$Y^d_{pj} = Yh_j|_{r=r_p} = \frac{2\varrho_j}{Q}\sum_{q=0}^{Q}\varrho_q T_{2q}(r_j)\sum_{m=0}^{q}\tilde{Y}^d_{qm}T_{2m}(r_p), \tag{25b}$$

$$T^d_{lj} = XYh_j|_{r=r_l} = \frac{2\varrho_j}{Q}\sum_{q=0}^{Q}\sum_{m=0}^{q}\sum_{n=0}^{m}\varrho_q T_{2q}(r_j)\tilde{Y}^d_{qm}\tilde{X}^d_{mn}T_{2n}(r_l). \tag{25c}$$

Multiplying X^d by Y^d and taking into account Eqs. (25a), (25b) we have

$$(X^dY^d)_{lj} = \sum_{p=0}^{Q}X^d_{lp}Y^d_{pj}$$

$$= \frac{2\varrho_j}{Q}\sum_{q=0}^{Q}\sum_{m=0}^{q}\sum_{q'=0}^{Q}\sum_{n=0}^{q'}\tilde{X}^d_{q'n}T_{2n}(r_l)\varrho_q T_{2q}(r_j)\tilde{Y}^d_{qm}\left[\frac{2\varrho_{q'}}{Q}\sum_{p=0}^{Q}\varrho_p T_{2q'}(r_p)T_{2m}(r_p)\right].$$

Since the expression in square brackets equals $\delta_{q'm}$ it follows that

$$(X^dY^d)_{lj} = \frac{2\varrho_j}{Q}\sum_{q=0}^{Q}\sum_{m=0}^{q}\sum_{n=0}^{m}\varrho_q T_{2q}(r_j)\tilde{Y}^d_{qm}\tilde{X}^d_{mn}T_{2n}(r_l). \tag{26}$$

Comparing Eqs. (25c) and (26) we obtain

$$T^d = X^dY^d.$$

This completes the proof of a theorem.

One can easily deduce from Theorem 2 and formulas (19) and (23) the validity of matrix identities

$$H^fL^f = L^uH^f, \qquad H^gL^g = L^uH^g, \tag{27a}$$

$$H^fR^f = H^gR^g = L^u + \alpha_m^2E, \tag{27b}$$

and, finally, the validity of relations (24).

D. *Discrete Poisson Equation for Pressure*

We now wish to use (24) to reduce Eqs. (21) to the form with almost decoupled grid functions $\mathbf{P}$, $\mathbf{F}$, $\mathbf{G}$, $\mathbf{U}$ and tau terms τ^f, τ^g, τ^u. In this section we consider the case $\alpha_m, n > 0$;

equations corresponding to $n=0$ and $\alpha_m=0$ may be easily derived using additional formulas of Appendix B.

We operate with H^f, H^g and $\partial/\partial x$ on Eqs. (21a), (21b), and (21c), respectively. Summing up the results and taking into account Eqs. (21d) we obtain then

$$L^u\mathbf{P}|_l = \frac{\partial}{\partial x}a_l^u + \frac{1}{2}H^f\mathbf{a}^f|_l + \frac{1}{2}H^g\mathbf{a}^g|_l + \frac{1}{2}\tau_0^f H_{l0}^f + \frac{1}{2}\tau_Q^f(1-\delta_{n1})H_{lQ}^f + \frac{1}{2}\tau_0^g H_{l0}^g + \frac{1}{2}\tau_Q^g(1-\delta_{n1}-\delta_{n2}-\delta_{n3})H_{lQ}^g,$$

$$l=1,2,\ldots,Q\ (n=1), \qquad l=1,2,\ldots,Q-1\ (n>1), \tag{28a}$$

$$H^f\mathbf{F}|_{l=0} + H^g\mathbf{G}|_{l=0} = 0, \qquad P_Q = 0\ (n>1),$$

where $\mathbf{a}^f \stackrel{\text{def}}{=} (a_0^f, a_1^f, \ldots, a_Q^f)^T$ and analogously for $\mathbf{a}^g$. Supplementing these equations by the ones following from (21)

$$\left(\frac{2}{\Delta t} - \nu L^f\right)\mathbf{F}|_l + R^f\mathbf{P}|_l = a_l^f + \tau_0^f\delta_{l0} + \tau_Q^f(1-\delta_{n1})\delta_{lQ}, \tag{28b}$$

$$l=0,1,\ldots,Q, \qquad F_0=0, \qquad F_Q=0\ (n>1)$$

$$\left(\frac{2}{\Delta t} - \nu L^g\right)\mathbf{G}|_l + R^g\mathbf{P}|_l = a_l^g + \tau_0^g\delta_{l0} + \tau_Q^g(1-\delta_{n1}-\delta_{n2}-\delta_{n3})\delta_{lQ}, \tag{28c}$$

$$l=0,1,\ldots,Q, \qquad G_0=0, \qquad G_Q=0\ (n>3)$$

$$\frac{\partial}{\partial x}U_l = -\frac{1}{2}H^f\mathbf{F}|_l - \frac{1}{2}H^g\mathbf{G}|_l, \qquad l=\begin{cases}0,1,\ldots,Q, & n=1\\ 0,1,\ldots,Q-1, & n>1,\end{cases} \tag{28d}$$

$$U_0=0, \qquad U_Q=0\ (n>1),$$

we obtain the set of Eqs. (28) equivalent to (21) and allowing the solution by means of the efficient influence matrix technique with tau correction [21]. However, when applying this technique to (28) we are faced with certain peculiarities. We briefly discuss the situation in Section VII.

For the discretization in φ and x we make use of Galerkin trigonometric approximation. In this case the unknown quantities are $\mathbf{q}_{nml}^{(i)}(t)$, $i=1,2,3,4$ —the values of Fourier coefficients in collocation nodes r_l,

$$\mathbf{q}_{nm}(r_l,\varphi,x,t) = \left(\mathbf{q}_{nml}^{(1)}\cos\alpha_m x + \mathbf{q}_{nml}^{(3)}\sin\alpha_m x\right)\cos n\varphi + \left(\mathbf{q}_{nml}^{(2)}\cos\alpha_m x + \mathbf{q}_{nml}^{(4)}\sin\alpha_m x\right)\sin n\varphi,$$

and analogously for $p_{nml}^{(i)}(t)$ and components of nonlinearity $(d^{u,f,g})_{nml}^{(i)}(t)$.

It should be stressed that the reduction of Eqs. (21) to the form (28) became possible just due to the new change of variables (12). Otherwise, the differential operators of Eqs. (14) and corresponding collocation matrices $L^{f,g,u}$, $H^{f,g}$, $R^{f,g}$ may have a form not satisfying relations (27), (24). As a result, the right hand side of Eq. (28a) will be the function of unknown values $\mathbf{F}^{k+1}$, $\mathbf{G}^{k+1}$, and $\mathbf{U}^{k+1}$, the decoupling of $\mathbf{F}$, $\mathbf{G}$, $\mathbf{U}$, and $\mathbf{P}$ will not happen, and there will be no opportunity to use influence matrices. Certainly, the aforesaid is true only if an implicit scheme is utilized for the viscous terms of Navier–Stokes equations. With an explicit treatment of viscous terms one can make use of much simpler solution procedures [7]. However, the latter essentially changes the stability boundary of the scheme.

An overall algorithm efficiency depends not only on the quality of a discrete Navier–Stokes solver but also on the availability of a fast and accurate method for the evaluation of nonlinear terms $d_{nml}^{f,g,u}$ in Eqs. (22). Such an algorithm was developed and we present it in the following section.

VI. FAST AND ACCURATE COMPUTATION OF NONLINEAR TERMS

The calculation of nonlinear terms $d_{nm}^{f,g,u}$ defined by (15) may be ill-conditioned when $r \to 0$. Negative powers of r also occur in the formulas for vorticity components necessary for the D^v, D^w, and D^u evaluation. Nevertheless, the algorithm presented below allows us to perform fast calculations of the Navier–Stokes nonlinear terms without loss of accuracy.

Boundedness and smoothness of functions $d_{nm}^{f,g,u}$ (the requirement for high accuracy calculations) follows directly from Eqs. (13a), (14), from the asymptotics of new variables at $r \to 0$ (Eqs. (9), (12)), and from axis conditions (13d). To avoid singularities the new algorithm exploits D_{nm}^u, $D_{nm}^v + \frac{1}{n}\frac{\partial}{\partial\varphi} D_{nm}^w$, and $D_{nm}^v - \frac{1}{n}\frac{\partial}{\partial\varphi} D_{nm}^w$ representations as a series of positive powers of r. More exactly, the primary terms of such representations are explicitly extracted and used then to avoid singularity problems in calculating the values of $d_{nm}^{f,g,u}$. Since each of the functions D_{nm}^u, D_{nm}^v, D_{nm}^w is expressed in terms of pairwise products of velocity and vorticity components the straightforward way to obtain the desired asymptotics is to evaluate directly the corresponding convolution sums. However, such an approach is of little use due to computational inefficiency. On the other hand, the routine implementation of a pseudospectral technique (that allows fast Fourier transforms to compute products) is completely useless since the behaviour of velocity and vorticity Fourier coefficients at $r \to 0$ strongly depends on azimuthal wavenumbers (Corollary 2). Below we suggest a certain combination of spectral and pseudospectral approaches providing that the major amount of computations is carried out by means of fast transforms.

We clarify the key aspects of a new algorithm considering the calculation of Fourier coefficients $(d^u)_{nml}^{(i)}$, $m, n \geq 0$; $l = 0, 1, \ldots, Q$, $i = 1, 2, 3, 4$ corresponding to the streamwise component of nonlinearity. For this purpose we rewrite Eq. (10) in the form

$$\mathbf{v} = \sum_{n=0}^{N}\sum_{m=0}^{M} \mathbf{v}_{nm}(r,\varphi,x,t) = \sum_{n=0}^{N} \mathbf{v}_n^C(r,x,t)\cos n\varphi + \sum_{n=1}^{N} \mathbf{v}_n^S(r,x,t)\sin n\varphi. \quad (29)$$

Similarly, we introduce functions $\mathbf{q}_n^{C,S}(r,x,t)$, $(d^u)_n^{C,S}(r,x,t)$. With regard for (15) we can obtain then

$$D^u(r,\varphi,x,t) \stackrel{\text{def}}{=} v\omega_\varphi - w\omega_r = \sum_{n=0}^{N} r^{\sigma_n}\left((d^u)_n^C \cos n\varphi + (d^u)_n^S \sin n\varphi\right). \quad (30)$$

Next, we write v, w, ω_r, and ω_φ as

$$v = r\bar{v}_0^C + \overbrace{\bar{v}_1^C\cos\varphi + \bar{v}_1^S\sin\varphi}^{A_1} + r\overbrace{\sum_{n=2}^{N} r^{\sigma_n}\left(\bar{v}_n^C\cos n\varphi + \bar{v}_n^S\sin n\varphi\right)}^{A_2}, \quad (31a)$$

$$\omega_\varphi = r(\bar{\omega}_\varphi)_0^C + \underbrace{a^C\cos\varphi + a^S\sin\varphi}_{B_1} + r\underbrace{\sum_{n=1}^{N} r^{\sigma_n}\left((\bar{\omega}_\varphi)_n^C\cos n\varphi + (\bar{\omega}_\varphi)_n^S\sin n\varphi\right)}_{B_2}, \quad (31b)$$

and analogously

$$w = r\bar{w}_0^C + A_3 + rA_4, \qquad \omega_r = r(\bar{\omega}_r)_0^C + B_3 + rB_4, \tag{31c}$$

where A_3 and A_4 result from A_1, A_2 by replacing $\bar{v}_n^{C,S}$ onto $\bar{w}_n^{C,S}$, B_4 from B_2 by replacing $(\bar{\omega}_\varphi)_n^{C,S}$ onto $(\bar{\omega}_r)_n^{C,S}$, and $B_3 = -a^S\cos\varphi + a^C\sin\varphi$. Here $\bar{v}_n^{C,S}(r,x,t)$, $\bar{w}_n^{C,S}(r,x,t)$, $(\bar{\omega}_r)_n^{C,S}(r,x,t)$, $(\bar{\omega}_\varphi)_n^{C,S}(r,x,t)$, $a^C(r,x,t)$, and $a^S(r,x,t)$ are smooth regular functions of the r-variable defined by the formulas

$$\begin{gathered}
\bar{v}_0^C = \tilde{v}_0^C, \qquad \bar{v}_n^{C,S} = \frac{1}{2}\bigl(r^{2\delta_{n1}}\tilde{f}_n^{C,S} + \tilde{g}_n^{C,S}\bigr),\\
\bar{w}_0^C = \tilde{w}_0^C, \qquad \bar{w}_n^{C,S} = \frac{1}{2}\bigl(\mp r^{2\delta_{n1}}\tilde{f}_n^{S,C} \pm \tilde{g}_n^{S,C}\bigr),\\
a^{C,S} = -\tilde{u}_1^{C,S} + \frac{1}{2}\frac{\partial}{\partial x}\tilde{g}_1^{C,S},\\
(\bar{\omega}_r)_0^C = -\frac{\partial}{\partial x}\tilde{w}_0^C, \qquad (\bar{\omega}_r)_1^{C,S} = \pm\frac{1}{2}\frac{\partial}{\partial x}\tilde{f}_1^{S,C},\\
(\bar{\omega}_r)_n^{C,S} = \pm n\frac{\tilde{u}_n^{S,C}}{r^2} \pm \frac{1}{2}\frac{\partial}{\partial x}\bigl(\tilde{f}_n^{S,C} - \tilde{g}_n^{S,C}\bigr),\\
(\bar{\omega}_\varphi)_0^C = \frac{\partial}{\partial x}\tilde{v}_0^C - \frac{1}{r}\frac{\partial}{\partial r}\tilde{u}_0^C, \qquad (\bar{\omega}_\varphi)_1^{C,S} = \frac{1}{2}\frac{\partial}{\partial x}\tilde{f}_1^{C,S} - \frac{1}{r}\frac{\partial}{\partial r}\tilde{u}_1^{C,S},\\
(\bar{\omega}_\varphi)_n^{C,S} = \frac{1}{2}\frac{\partial}{\partial x}\bigl(\tilde{f}_n^{C,S} + \tilde{g}_n^{C,S}\bigr) - \sigma_n\frac{\tilde{u}_n^{C,S}}{r^2} - \frac{1}{r}\frac{\partial}{\partial r}\tilde{u}_n^{C,S}.
\end{gathered} \tag{32}$$

By substituting expressions (31) into Eq. (30) we directly obtain

$$\begin{aligned}
(d^u)_0^C(r,x,t) &= \frac{1}{2}a^C\bigl(\bar{v}_1^C - \bar{w}_1^S\bigr) + \frac{1}{2}a^S\bigl(\bar{v}_1^S + \bar{w}_1^C\bigr)\\
&\quad + r\bigl((C_{12})_0^C + (C_{21})_0^C - (C_{34})_0^C - (C_{43})_0^C\bigr)\\
&\quad + r^2\bigl(\bar{v}_0^C(\bar{\omega}_\varphi)_0^C - \bar{w}_0^C(\bar{\omega}_r)_0^C + (C_{22})_0^C - (C_{44})_0^C\bigr),
\end{aligned} \tag{33a}$$

$$\begin{aligned}
(d^u)_n^{C,S}(r,x,t) &= \delta_{n1}\bigl(a^{C,S}\bar{v}_0^C \pm a^{S,C}\bar{w}_0^C + \bar{v}_1^{C,S}(\bar{\omega}_\varphi)_0^C - \bar{w}_1^{C,S}(\bar{\omega}_r)_0^C\bigr)\\
&\quad + (1-\delta_{n1})r^2\bigl(\bar{v}_n^{C,S}(\bar{\omega}_\varphi)_0^C - \bar{w}_n^{C,S}(\bar{\omega}_r)_0^C\bigr)\\
&\quad + \frac{1}{2}\delta_{n2}\bigl(a^{C,S}\bigl(\bar{v}_1^C + \bar{w}_1^S\bigr) \mp a^{S,C}\bigl(\bar{v}_1^S - \bar{w}_1^C\bigr)\bigr) + r^2\bigl((\bar{\omega}_\varphi)_n^{C,S}\bar{v}_0^C - (\bar{\omega}_r)_n^{C,S}\bar{w}_0^C\bigr)\\
&\quad + r^{1-\sigma_n}\bigl((C_{12})_n^{C,S} + (C_{21})_n^{C,S} + r(C_{22})_n^{C,S} - (C_{34})_n^{C,S}\\
&\quad - (C_{43})_n^{C,S} - r(C_{44})_n^{C,S}\bigr), \qquad n = 1,2,\ldots,N,
\end{aligned} \tag{33b}$$

where functions $(C_{ij})_n^{C,S}(r,x,t)$ are defined by the relations

$$\sum_{n=0}^{2N}(C_{ij})_n^C\cos n\varphi + \sum_{n=1}^{2N}(C_{ij})_n^S\sin n\varphi = A_iB_j. \tag{34}$$

From (34) and the explicit form of functions A_i, B_j it follows that almost all functions $(C_{ij})_n^{C,S}$ of Eqs. (33) may be calculated by means of simple formulas with a minimal number

of arithmetic operations involved. For example, from Eqs. (31) and (34) it follows that

$$(C_{12})_n^C = \frac{1}{2} r^{1-\sigma_n} \left(\overline{v}_1^C (\overline{\omega}_\varphi)_{n-1}^C - \overline{v}_1^S (\overline{\omega}_\varphi)_{n-1}^S \right) (1 - \delta_{n0} - \delta_{n1})$$

$$+ \frac{1}{2} r^{1-\sigma_n} \left(\overline{v}_1^C (\overline{\omega}_\varphi)_{n+1}^C + \overline{v}_1^S (\overline{\omega}_\varphi)_{n+1}^S \right) (1 - \delta_{nN}), \tag{35}$$

and similar formulas for $(C_{12})_n^S$, $(C_{21})_n^{C,S}$, $(C_{34})_n^{C,S}$, and $(C_{43})_n^{C,S}$. As to functions $(C_{22})_n^{C,S}$ and $(C_{44})_n^{C,S}$, an ordinary pseudospectral technique with the 3/2-rule to avoid aliasing may be utilized.

Summarizing, we suggest the following computational procedure for the Fourier coefficients of nonlinearity:

(1) Using $\mathbf{q}_{nml}^{(i)}$ we compute the values of functions $\mathbf{q}_n^{C,S}(r, x, t)$ at the set of points $r_l = R \cos(\pi l / 2Q)$, $l = 0, 1, \ldots, Q$; $x_i = iX/2M_*$, $i = -M_* + 1, -M_* + 2, \ldots, M_*$, $2M_* \geq 3M + 1$:

$$\begin{pmatrix} \mathbf{q}_n^C \\ \mathbf{q}_n^S \end{pmatrix} (r_l, x_i, t) = \sum_{m=0}^{M} \left[\begin{pmatrix} \mathbf{q}_{nml}^{(1)} \\ \mathbf{q}_{nml}^{(2)} \end{pmatrix} \cos \frac{\pi m i}{M_*} + \begin{pmatrix} \mathbf{q}_{nml}^{(3)} \\ \mathbf{q}_{nml}^{(4)} \end{pmatrix} \sin \frac{\pi m i}{M_*} \right]. \tag{36}$$

(2) Using discrete analogues to relations (32) we calculate the values of functions $\overline{v}_n^{C,S}$, $\overline{w}_n^{C,S}$, $(\overline{\omega}_r)_n^{C,S}$, $(\overline{\omega}_\varphi)_n^{C,S}$, $a^{C,S}$. For example,

$$(\overline{\omega}_r)_n^C (r_l, x_i, t) = n \sum_{j=0}^{Q} S_{lj} \tilde{u}_n^s (r_j, x_i, t)$$

$$+ \frac{1}{2} \sum_{m=0}^{M} \left(-\alpha_m \left(\tilde{f}_{nml}^{(2)} - \tilde{g}_{nml}^{(2)} \right) \sin \frac{\pi m i}{M_*} + \alpha_m \left(\tilde{f}_{nml}^{(4)} - \tilde{g}_{nml}^{(4)} \right) \cos \frac{\pi m i}{M_*} \right), \qquad n > 1. \tag{37}$$

Note that discrete Fourier transforms in (36), (37) may be evaluated by the Fast Fourier Transform algorithm.

(3) Next, $(d^u)_n^{C,S}(r_l, x_i, t)$, $n = 0, 1, \ldots, N$ are calculated according to (33).

(4) The desired Fourier coefficients $(d^u)_{nml}^{(i)}$ are obtained finally by means of the inverse discrete Fourier transform.

In addition, we briefly consider the evaluation of d^f and d^g components of nonlinearity. Similarly to (31) we represent the streamwise components of velocity and vorticity in the form

$$\begin{pmatrix} u \\ \omega_x \end{pmatrix} = \begin{pmatrix} \overline{u}_0^C \\ (\overline{\omega}_x)_0^C \end{pmatrix} + r \left[\begin{pmatrix} \overline{u}_1^C \\ (\overline{\omega}_x)_1^C \end{pmatrix} \cos \varphi + \begin{pmatrix} \overline{u}_1^S \\ (\overline{\omega}_x)_1^S \end{pmatrix} \sin \varphi \right]$$

$$+ r^2 \sum_{n=2}^{N} r^{\sigma_n} \left[\begin{pmatrix} \overline{u}_n^C \\ (\overline{\omega}_x)_n^C \end{pmatrix} \cos n\varphi + \begin{pmatrix} \overline{u}_n^S \\ (\overline{\omega}_x)_n^S \end{pmatrix} \sin n\varphi \right], \tag{38}$$

where

$$\overline{u}_0^C = \tilde{u}_0^C, \qquad \overline{u}_1^{C,S} = \tilde{u}_1^{C,S}, \qquad \overline{u}_n^{C,S} = \frac{\tilde{u}_n^{C,S}}{r^2},$$

$$(\overline{\omega}_x)_0^C = 2\tilde{w}_0^C + r \frac{\partial}{\partial r} \tilde{w}_0^C, \qquad (\overline{\omega}_x)_1^{C,S} = \mp \frac{1}{2} \left(4 \tilde{f}_1^{S,C} + r \frac{\partial}{\partial r} \tilde{f}_1^{S,C} - \frac{1}{r} \frac{\partial}{\partial r} \tilde{g}_1^{S,C} \right), \tag{39}$$

$$(\overline{\omega}_x)_n^{C,S} = \mp \frac{1}{2} \left(\frac{\tilde{f}_n^{S,C}}{r^2} (n + \sigma_n + 2) + \frac{\tilde{g}_n^{S,C}}{r^2} (n - \sigma_n - 2) + \frac{1}{r} \frac{\partial}{\partial r} \tilde{f}_n^{S,C} - \frac{1}{r} \frac{\partial}{\partial r} \tilde{g}_n^{S,C} \right), \qquad n > 1.$$

We stress that analogously (32), formulas (39) define smooth regular functions of the r-variable. As it follows from axis conditions (13d) and Eqs. (18) the evaluation of these functions may be carried out without any loss of accuracy.

According to (31) and (38) we obtain

$$\begin{pmatrix} D^v \\ D^w \end{pmatrix} \stackrel{\text{def}}{=} \begin{pmatrix} w\omega_x - u\omega_\varphi \\ u\omega_r - v\omega_x \end{pmatrix} = \begin{pmatrix} \overline{w}_1^C(\overline{\omega}_x)_0^C - a^C\overline{u}_0^C \\ -\overline{v}_1^C(\overline{\omega}_x)_0^C - a^S\overline{u}_0^C \end{pmatrix}\cos\varphi + \begin{pmatrix} \overline{w}_1^S(\overline{\omega}_x)_0^C - a^S\overline{u}_0^C \\ -\overline{v}_1^S(\overline{\omega}_x)_0^C + a^C\overline{u}_0^C \end{pmatrix}\sin\varphi$$
$$+ \sum_{n=0}^{N} r^{\sigma_n+1}\left[\begin{pmatrix} (d^v)_n^C \\ (d^w)_n^C \end{pmatrix}\cos n\varphi + \begin{pmatrix} (d^v)_n^S \\ (d^w)_n^S \end{pmatrix}\sin n\varphi \right], \tag{40}$$

where $(d^v)_n^{C,S}$ and $(d^w)_n^{C,S}$ are defined by formulas similar to (33). As to functions $(d^f)_n^{C,S}$ and $(d^g)_n^{C,S}$ it follows according to (15) that

$$\begin{aligned}
(d^f)_1^{C,S} &= (d^v)_1^{C,S} \pm (d^w)_1^{S,C} \mp (\overline{\omega}_x)_0^C\,\tilde{f}_1^{S,C}, \\
(d^f)_n^{C,S} &= (d^v)_n^{C,S} \pm (d^w)_n^{S,C}, \qquad n > 1, \\
(d^g)_1^{C,S} &= \pm(\overline{\omega}_x)_0^C\,\tilde{g}_1^{S,C} - 2a^{C,S}\overline{u}_0^C + r^2\big((d^v)_1^{C,S} \mp (d^w)_1^{S,C}\big), \\
(d^g)_n^{C,S} &= (d^v)_n^{C,S} \mp (d^w)_n^{S,C}, \qquad n > 1.
\end{aligned}$$

In all other respects the calculation of the desired Fourier coefficients $(d^f)_{nml}^{(i)}$ and $(d^g)_{nml}^{(i)}$ is analogous to the evaluation of $(d^u)_{nml}^{(i)}$ considered above.

VII. IMPLEMENTATION OF INFLUENCE MATRICES

An efficient solution procedure for the equations similar to (28) was originally suggested in Cartesian coordinates by Kleiser and Schumann [21]. Thereupon it was an object of modifications (see, e.g., [17, 23, 24]) and is known now as an influence matrix method with tau correction. However, Eqs. (28) possess certain peculiarities associated with distinct boundary conditions at various azimuthal wavenumbers. We briefly consider below the principal aspects of influence matrices implementation in this case. In what follows we limit ourselves to $\alpha_m, n > 0$. Equations corresponding to $\alpha_m = 0$ and $n = 0$ can be obtained in a similar way using formulas from Appendix B.

Solutions of Eqs. (28) we seek in the form

$$\begin{pmatrix} P_l \\ F_l \\ G_l \end{pmatrix} = \begin{pmatrix} P_l^1 \\ F_l^1 \\ G_l^1 \end{pmatrix} + \tau_0^f \begin{pmatrix} P_l^{2a} \\ F_l^{2a} \\ G_l^{2a} \end{pmatrix} + \tau_0^g \begin{pmatrix} P_l^{2b} \\ F_l^{2b} \\ G_l^{2b} \end{pmatrix} + \tau_Q^f(1-\delta_{n1}) \begin{pmatrix} P_l^{2c} \\ F_l^{2c} \\ G_l^{2c} \end{pmatrix}$$
$$+ \tau_Q^g(1-\delta_{n1}-\delta_{n2}-\delta_{n3}) \begin{pmatrix} P_l^{2d} \\ F_l^{2d} \\ G_l^{2d} \end{pmatrix} + P_0 \begin{pmatrix} P_l^3 \\ F_l^3 \\ G_l^3 \end{pmatrix}, \tag{41}$$
$$l = 1, 2, \ldots, Q_f \text{ for } P, F; \qquad l = 1, 2, \ldots, Q_g \text{ for } G,$$

where

$$Q_f \stackrel{\text{def}}{=} \begin{cases} Q, & n = 1 \\ Q-1, & n > 1; \end{cases} \qquad Q_g \stackrel{\text{def}}{=} \begin{cases} Q, & n = 1, 2, 3 \\ Q-1, & n > 3. \end{cases}$$

Vectors $\mathbf{P}^k \stackrel{\text{def}}{=} (P_0^k, P_1^k, \ldots, P_Q^k)^T$ as well as $\mathbf{F}^k, \mathbf{G}^k (k = 1, 2a, 2b, 2c, 2d, 3)$ are the solutions of the following discrete boundary-value problems:

$$\begin{gathered} L^u \mathbf{P}^1|_l = \frac{\partial}{\partial x} a_l^u + \frac{1}{2} H^f \mathbf{a}^f|_l + \frac{1}{2} H^g \mathbf{a}^g|_l, \qquad l = 1, 2, \ldots, Q_f, \\ P_0^1 = 0, \qquad P_Q^1 = 0 \ (n > 1), \end{gathered} \tag{42a}$$

$$\begin{gathered} \left(\frac{2}{\Delta t} E - \nu L^f \right) \mathbf{F}^1|_l = -R^f \mathbf{P}^1|_l + a_l^f, \qquad l = 1, 2, \ldots, Q_f, \\ F_0^1 = 0, \qquad F_Q^1 = 0 \ (n > 1), \end{gathered} \tag{42b}$$

$$\begin{gathered} \left(\frac{2}{\Delta t} E - \nu L^g \right) \mathbf{G}^1|_l = -R^g \mathbf{P}^1|_l + a_l^g, \qquad l = 1, 2, \ldots, Q_g, \\ G_0^1 = 0, \qquad G_Q^1 = 0 \ (n > 3); \end{gathered} \tag{42c}$$

$$\begin{gathered} L^u \mathbf{P}^k|_l = \tfrac{1}{2} S_l^k, \qquad l = 1, 2, \ldots, Q_f, \\ P_0^k = 0, \qquad P_Q^k = 0 \ (n > 1), \\ \left(\frac{2}{\Delta t} E - \nu L^f \right) \mathbf{F}^k|_l = -R^f \mathbf{P}^k|_l, \qquad l = 1, 2, \ldots, Q_f, \\ F_0^k = 0, \qquad F_Q^k = 0 \ (n > 1), \\ \left(\frac{2}{\Delta t} E - \nu L^g \right) \mathbf{G}^k|_l = -R^g \mathbf{P}^k|_l, \qquad l = 1, 2, \ldots, Q_g, \\ G_0^k = 0, \qquad G_Q^k = 0 \ (n > 3), \end{gathered} \tag{43}$$

where k takes the values $2a, 2b, 2c, 2d$ and $S_l^{2a} = H_{l0}^f$, $S_l^{2b} = H_{l0}^g$, $S_l^{2c} = H_{lQ}^f$, $S_l^{2d} = H_{lQ}^g$;

$$\begin{gathered} L^u \mathbf{P}^3|_l = 0, \qquad l = 1, 2, \ldots, Q_f, \\ P_0^3 = 1, \qquad P_Q^3 = 0 \ (n > 1), \\ \left(\frac{2}{\Delta t} E - \nu L^f \right) \mathbf{F}^3|_l = -R^f \mathbf{P}^3|_l, \qquad l = 1, 2, \ldots, Q_f, \\ F_0^3 = 0, \qquad F_Q^3 = 0 \ (n > 1), \\ \left(\frac{2}{\Delta t} E - \nu L^g \right) \mathbf{G}^3|_l = -R^g \mathbf{P}^3|_l, \qquad l = 1, 2, \ldots, Q_g, \\ G_0^3 = 0, \qquad G_Q^3 = 0 \ (n > 3). \end{gathered} \tag{44}$$

The unknown coefficients τ_0^f, τ_Q^f, τ_0^g, τ_Q^g, and P_0 (the latter being the value of the total pressure Fourier coefficient on a pipe wall) can be evaluated from

$$H^f \mathbf{F}|_{l=0} + H^g \mathbf{G}|_{l=0} = 0, \qquad n > 0, \tag{45a}$$

$$-\nu L^f \mathbf{F}|_{l=0} + R^f \mathbf{P}|_{l=0} - \tau_0^f - a_0^f = 0, \qquad n > 0, \tag{45b}$$

$$-\nu L^g \mathbf{G}|_{l=0} + R^g \mathbf{P}|_{l=0} - \tau_0^g - a_0^g = 0, \qquad n > 0, \tag{45c}$$

$$-\nu L^f \mathbf{F}|_{l=Q} + R^f \mathbf{P}|_{l=Q} - \tau_Q^f - a_Q^f = 0, \qquad n > 1, \tag{45d}$$

$$-\nu L^g \mathbf{G}|_{l=Q} + R^g \mathbf{P}|_{l=Q} - \tau_Q^g - a_Q^g = 0, \qquad n > 3. \tag{45e}$$

Equations (45) directly follow from (28). In case $n = 1$ the necessary parameters τ_0^f, τ_0^g, and P_0 are evaluated from the first three of them. For $n = 2, 3$ the desired τ_0^f, τ_0^g, τ_Q^f, P_0 can

be obtained as a solutions of Eqs. (45a)–(45d). When $n > 3$ we calculate τ_0^f, τ_0^g, τ_Q^f, τ_Q^g, and P_0 by means of all five equations (45).

Equations (45) have to be resolved at each timestep and iteration loop. They may be reduced to the form

$$A\mathbf{x} = \mathbf{b},$$

where $\mathbf{x} = (\tau_0^f, \tau_0^g, \tau_Q^f, \tau_Q^g, P_0)^T$, A is the constant matrix (its own for each pair of wavenumbers (m, n)) and the right side $\mathbf{b}$ depends on time being the function of $\mathbf{F}^1$, $\mathbf{G}^1$, $\mathbf{P}^1$. Matrices A^{-1} (their maximum order equals 5) may be evaluated only once in a pre-processing step. The same is true for grid functions $\mathbf{F}^k$, $\mathbf{G}^k$, and $\mathbf{P}^k$, $k = 2a, 2b, 2c, 2d, 3$—the solutions of Eqs. (43), (44).

Similarly to (45), Eqs. (42) must be solved at each timestep. An explicit form of matrices L^u, $(2/\Delta t - \nu L^f)$ and $(2/\Delta t - \nu L^g)$ (see Eqs. (23)) allows one to exploit for this purpose an efficient collocation-diagonalization technique [25].

VIII. NUMERICAL RESULTS

Numerical verification of the algorithm includes two issues. First, we compare spectral characteristics of the pipe Poiseuille flow stability problem with those of the discrete linearized Navier–Stokes operator. Second, we present results of direct Navier–Stokes simulation of laminar-turbulent transition in a circular pipe at Reynolds number $Re = \bar{U} D/\nu = 4000$, based on the mean velocity (see also Eq. (3c)) and pipe diameter $D = 2R$. In this section, unless otherwise stipulated, the centreline velocity of parabolic base flow and pipe radius R are used as units of velocity and length. Computations were carried out on the Hewlett Packard VECTRA PC and Sun SPARCcenter 2000.

A. *Pipe Poiseuille Flow Linear Stability Problem*

Equations (13) have stationary solutions

$$\tilde{v}_{00} = \tilde{w}_{00} = 0, \qquad \tilde{u}_{00} = U^0(r) = 1 - r^2, \qquad p_x(t) = -4\nu, \qquad \tilde{p}_{00} = \frac{1}{2}(U^0)^2 + \text{const}, \tag{46}$$

which describe laminar fluid flows in $\mathcal{G}$.

We linearize (13) about arbitrary solution (46) neglecting the terms being quadratic with respect to disturbance amplitudes. In addition, it is convenient to exploit dependent variables $\mathbf{v}_{nm}^F(r, t)$ and $\mathbf{q}_{nm}^F(r, t)$ instead of functions $\mathbf{v}_{nm}(r, \varphi, x, t)$, $\mathbf{q}_{nm}(r, \varphi, x, t)$ (see Eq. (10)). Conducting spatial discretization as it was recommended in previous sections we obtain the following linear stability problem for pipe Poiseuille flow (for definiteness we consider below the case $\alpha_m \neq 0, n > 0$),

$$\bar{\lambda} F_l = -i\alpha_m U^0(r_l) F_l - R^f \mathbf{P}|_l + \nu L^f \mathbf{F}|_l + \tau_0^f \delta_{l0} + \tau_Q^f (1 - \delta_{n1}) \delta_{lQ}, \tag{47a}$$

$$l = 0, 1, \ldots, Q, \qquad F_0 = 0, \qquad F_Q = 0 \ (n > 1)$$

$$\bar{\lambda} G_l = -i\alpha_m U^0(r_l) G_l - R^g \mathbf{P}|_l + \nu L^g \mathbf{G}|_l + \tau_0^g \delta_{l0} + \tau_Q^g (1 - \delta_{n1} - \delta_{n2} - \delta_{n3}) \delta_{lQ}, \tag{47b}$$

$$l = 0, 1, \ldots, Q, \qquad G_0 = 0, \qquad G_Q = 0 \ (n > 3)$$

$$\bar{\lambda} U_l = -i\alpha_m U^0(r_l) U_l + \left(r_l^2 F_l + a_l G_l\right) - i\alpha_m P_l + \nu L^u \mathbf{U}|_l + \tau_0^u \delta_{l0} + \tau_Q^u (1 - \delta_{n1}) \delta_{lQ}, \tag{47c}$$

$$l = 0, 1, \ldots, Q, \qquad U_0 = 0, \qquad U_Q = 0 \ (n > 1)$$

$$H^f \mathbf{F}|_l + H^g \mathbf{G}|_l + 2i\alpha_m U_l = 0, \qquad l = 0, 1, \ldots, Q_f, \qquad P_Q = 0 \ (n > 1), \tag{47d}$$

where $\nu = 1/Re$; $a_l = 1$ $(n = 1)$, $a_l = r_l^2$ $(n > 1)$; Q_f is defined in (41); **F**, **G**, **U**, **P** are the disturbances of the base flow (46) corresponding to wavenumbers α_m, n: $\mathbf{F} = (F_0, F_1, \ldots, F_Q)^T$, $F_l = e^{-\bar{\lambda} t} \tilde{f}^F_{nm}(r_l, t)$ and analogously for **G**, **U**, **P**.

Equations (47) determine stability characteristics of pipe Poiseuille flow in the linear approach. Once these equations are reduced to the standard form

$$\bar{\lambda} \mathbf{x} = \bar{T} \mathbf{x}, \tag{48}$$

eigenvalues $\bar{\lambda}$ and eigenvectors **x** may be found by means of the QR algorithm. The finite set $\bar{\lambda}_k = \bar{\lambda}_k(\alpha_m, n, Re, Q)$, $re\bar{\lambda}_k \geq re\bar{\lambda}_{k+1}$, $k = 1, 2, \ldots, K < \infty$ is usually considered as an approximation to *a priori* unknown eigenvalues $\lambda_k(\alpha_m, n, Re)$, $k = 1, 2, \ldots$ of the differential problem.

Reduction of Eqs. (47) to the canonical form (48) is an important stage of the solution procedure. Below we consider a reduction algorithm that is economical and weakly sensitive to the round-off errors. As far as we known, similar algorithms were not used before, even in Cartesian coordinates where the implementation of influence matrices is straightforward.

We multiply Eq. (47c) by $2i\alpha_m$ and operate with matrices H^f, H^g on Eqs. (47a), (47b), respectively. Summing up the results we obtain (making use of Eq. (47d) and matrix identities (24)) the following discrete Poisson equation for pressure:

$$\begin{aligned} L^u \mathbf{P}|_l = {} & \alpha_m^2 U^0(r_l) U_l - \frac{1}{2} i\alpha_m \sum_{j=0}^{Q} \left(H^f_{lj} U^0(r_j) F_j + H^g_{lj} U^0(r_j) G_j\right) \\ & + i\alpha_m \left(r_l^2 F_l + a_l G_l\right) + \frac{1}{2}\tau_0^f H^f_{l0} + \frac{1}{2}\tau_Q^f (1 - \delta_{n1}) H^f_{lQ} \\ & + \frac{1}{2}\tau_0^g H^g_{l0} + \frac{1}{2}\tau_Q^g (1 - \delta_{n1} - \delta_{n2} - \delta_{n3}) H^g_{lQ}, \qquad l = 1, 2, \ldots, Q_f. \end{aligned} \tag{49}$$

To express **U** and tau terms τ_0^f, τ_Q^f, τ_0^g, τ_Q^g through **F**, **G**, and **P** we utilize Eqs. (47a), (47b) for $l = 0$, Q and equalities (47d). After substituting the result into the right side of Eq. (49) and exploiting the remaining equations from (47a), (47b) we arrive at the equivalent spectral problem of the form

$$\hat{L}^u \mathbf{P}|_l = A^f \mathbf{F}|_l + A^g \mathbf{G}|_l, \qquad l = 1, 2, \ldots, Q_f, \qquad (H^f \mathbf{F} + H^g \mathbf{G})|_{l=0} = 0, \qquad P_Q = 0 \ (n > 1), \tag{50a}$$

$$\bar{\lambda} F_l = -i\alpha_m U^0(r_l) F_l - R^f \mathbf{P}|_l + \nu L^f \mathbf{F}|_l, \qquad l = 1, 2, \ldots, Q_f, \qquad F_0 = 0, \qquad F_Q = 0 \ (n > 1) \tag{50b}$$

$$\bar{\lambda}G_l = -i\alpha_m U^0(r_l)G_l - R^g\mathbf{P}|_l + \nu L^g\mathbf{G}|_l, \qquad l = 1, 2, \ldots, Q_g,$$
$$G_0 = 0, \qquad G_Q = 0 \ (n > 3). \tag{50c}$$

Here $\hat{L}^u$ is a real and A^f, A^g are complex-valued $(Q+1)\times(Q+1)$ matrices.

Solutions of Eqs. (50) we suggest to seek in the form

$$\begin{pmatrix}\mathbf{F}\\ \mathbf{G}\end{pmatrix} = \begin{pmatrix}\mathbf{F}^1\\ \mathbf{G}^1\end{pmatrix} + \begin{pmatrix}\mathbf{F}^2\\ \mathbf{G}^2\end{pmatrix},$$

where $\mathbf{F}^1$, $\mathbf{G}^1$ satisfy Eqs. (51),

$$\hat{L}^u\mathbf{P}^1|_l = A^f\mathbf{F}|_l + A^g\mathbf{G}|_l, \qquad l = 1, 2, \ldots, Q_f,$$
$$P_0^1 = 0, \qquad P_Q^1 = 0 \ (n > 1) \tag{51a}$$

$$\bar{\lambda}F_l^1 = (-i\alpha_m U^0(r_l)F_l + \nu L^f\mathbf{F}|_l) - R^f\mathbf{P}^1|_l, \qquad l = 1, 2, \ldots, Q_f,$$
$$F_0^1 = 0, \qquad F_Q^1 = 0 \ (n > 1) \tag{51b}$$

$$\bar{\lambda}G_l^1 = (-i\alpha_m U^0(r_l)G_l + \nu L^g\mathbf{G}|_l) - R^g\mathbf{P}^1|_l, \qquad l = 1, 2, \ldots, Q_g,$$
$$G_0^1 = 0, \qquad G_Q^1 = 0 \ (n > 3) \tag{51c}$$

and $\mathbf{F}^2$, $\mathbf{G}^2$ are the solutions of

$$\hat{L}^u\mathbf{P}^2|_l = 0, \qquad l = 1, 2, \ldots, Q_f, \tag{52a}$$

$$(H^f\mathbf{F} + H^g\mathbf{G})|_{l=0} = 0, \qquad P_Q^2 = 0 \ (n > 1), \tag{52b}$$

$$\bar{\lambda}F_l^2 = -R^f\mathbf{P}^2|_l, \qquad l = 1, 2, \ldots, Q_f,$$
$$F_0^2 = 0, \qquad F_Q^2 = 0 \ (n > 1), \tag{52c}$$

$$\bar{\lambda}G_l^2 = -R^g\mathbf{P}^2|_l, \qquad l = 1, 2, \ldots, Q_g,$$
$$G_0^2 = 0, \qquad G_Q^2 = 0 \ (n > 3). \tag{52d}$$

Next, we express $\mathbf{P}^1$ through $\mathbf{F}$ and $\mathbf{G}$ by means of Eq. (51a) and substitute the result into the right hand side of equalities (51b), (51c). Thus, we obtain $\bar{\lambda}\mathbf{F}^1$, $\bar{\lambda}\mathbf{G}^1$ as the functions of $\mathbf{F}$ and $\mathbf{G}$. Similarly, the relation between $\bar{\lambda}\mathbf{F}^2$, $\bar{\lambda}\mathbf{G}^2$ and $\mathbf{F}$, $\mathbf{G}$ is given by the relations

$$\bar{\lambda}F_l^2 = -\kappa R^f\mathbf{h}|_l, \qquad l = 1, 2, \ldots, Q_f,$$
$$\bar{\lambda}G_l^2 = -\kappa R^g\mathbf{h}|_l, \qquad l = 1, 2, \ldots, Q_g,$$

where vector $\mathbf{h} = (h_0, h_1, \ldots, h_Q)^T$ is the solution of a problem

$$\hat{L}^u\mathbf{h}|_l = 0, \qquad l = 1, 2, \ldots, Q_f,$$
$$h_0 = 1, \quad h_Q = 0 \ (n > 1).$$

Coefficient κ as a function of $\mathbf{F}^1$, $\mathbf{G}^1$ (and via $\mathbf{F}^1$, $\mathbf{G}^1$ as a function of $\mathbf{F}$, $\mathbf{G}$) can be evaluated from

$$(H^f\mathbf{F}^2 + H^g\mathbf{G}^2)|_{l=0} = -(H^f\mathbf{F}^1 + H^g\mathbf{G}^1)|_{l=0}.$$

As a result we obtain then

$$\bar{\lambda}\begin{pmatrix}\mathbf{F}\\ \mathbf{G}\end{pmatrix} = \bar{\lambda}\begin{pmatrix}\mathbf{F}^1+\mathbf{F}^2\\ \mathbf{G}^1+\mathbf{G}^2\end{pmatrix} = T\begin{pmatrix}\mathbf{F}\\ \mathbf{G}\end{pmatrix}, \tag{53}$$

where T is a certain complex $(Q_f + Q_g)\times(Q_f + Q_g)$ matrix. If we eliminate the F_1 component of vector $\mathbf{F}$ from (53) (components of $\mathbf{F}$ are linearly dependent according to the first equation of (52b)) we finally come to the spectral problem (48) with

$$\mathbf{x} = (F_2, F_3, \ldots, F_{Q_f}, G_1, G_2, \ldots, G_{Q_g})^T.$$

Table 1 illustrates exponential in Q convergence of the pseudospectral discretization used. Our results agree with those of [15] ($\lambda_1 = -0.023170795764 - i0.950481396668$) and [18] ($\lambda_1 = -0.023170795 - i0.950481397$). Data given in Table 1 correspond to high accuracy calculations with the roundoff error of about one part in 10^{35}. Notice also that the convergence rate of our algorithm is comparable with those of the spectral method [15, Table on p. 340].

Following previous authors (see, e.g., [12]) we agree that the computer roundoff errors should be distinguished from truncation ones. In Table 2 we show the effect of both types of them on the eigenvalues evaluated by means of our algorithm. Above all, we point to the extremely weak sensitivity of the algorithm to the roundoff errors. Indeed, from two to three true digits are permanently observed in the case of low precision (roundoff $\simeq 10^{-7}$) calculations for a wide range of numbers of collocation points. Note that $Q + 1 = 181$ corresponds to the interpolation polynomials (18) incorporating Chebyshev polynomials T_{2l}, $l = 0, 1, \ldots, Q$ of a very high (up to $2Q = 360$) order. These results are much better than the typical roundoff sensitivity of spectral methods illustrated by Orszag in [26, Table 3, p. 696].

We stress that weak sensitivity of the algorithm to roundoff errors at large Q is of special interest in the context of reliable approximation of Fourier modes with considerable streamwise and azimuthal wavenumbers. Table 3 illustrates the necessity to use much larger resolution for $\alpha_m, n \gg 1$: no one correct eigenvalue can be calculated with 31 collocation points compared to 7 true digits of $\bar{\lambda}_1$ at $\alpha_m = n = 1$ obtained with $Q + 1 = 21$ collocation nodes (Table 2). In addition, as it follows from Table 4, only three leading eigenvalues $\bar{\lambda}_k$, $k = 1, 2, 3$ can be properly calculated with 61 collocation points for $\alpha_m = n = 20$, even with 11 true digits for $\bar{\lambda}_1$ at the same resolution (Table 3)! Such behaviour must be taken

TABLE 1

Convergence of the Least Stable Eigenvalue for $Re = 9600$, $\alpha_m = n = 1$

Q + 1	re($\bar{\lambda}_1$)	im($\bar{\lambda}_1$)
21	−0.02318	−0.950497
26	−0.0231710	−0.9504815
31	−0.023170795	−0.9504813961
36	−0.023170795770	−0.950481396671
41	−0.02317079576499	−0.950481396669905
46	−0.02317079576500423	−0.950481396669903171
51	−0.023170795765004215199	−0.950481396669903179 50
56	−0.0231707957650042152055	−0.9504813966699031794843
61	−0.0231707957650042152055	−0.9504813966699031794843

TABLE 2
Influence of Round-Off Error on the Leading Eigenvalue $\bar{\lambda}_1$; $Re = 4000$, $\alpha_m = n = 1$

Q + 1	Roundoff $\simeq 10^{-7}$	Roundoff $\simeq 10^{-16}$	Roundoff $\simeq 10^{-35}$
21	$-0.0358 - 0.9233i$	$-0.0357935 - 0.9233155i$	$-0.03579355 - 0.9233155i$
31	$-0.0361 - 0.9233i$	$-0.035793677913 - 0.923314870453i$	$-0.035793677912 - 0.923314870454i$
41	$-0.0356 - 0.9233i$	$-0.035793677911 - 0.923314870452i$	$-0.035793677910732358 4 - 0.923314870451898520 28i$
51	$-0.0359 - 0.9233i$	$-0.035793677911 - 0.923314870452i$	$-0.035793677910732357 9865 - 0.923314870451898520 388i$
61	$-0.0358 - 0.9234i$	$-0.035793677911 - 0.923314870452i$	$-0.035793677910732357 9865 - 0.923314870451898520 3883i$
71	$-0.0361 - 0.9236i$	$-0.035793677911 - 0.923314870452i$	$-0.035793677910732357 9865 - 0.923314870451898520 3883i$
81	$-0.0357 - 0.9233i$	$-0.035793677911 - 0.923314870452i$	$-0.035793677910732357 9866 - 0.923314870451898520 3882i$
121	$-0.0355 - 0.9237i$	$-0.035793677909 - 0.923314870452i$	
181	$-0.0363 - 0.9246i$	$-0.035793677910 - 0.923314870451i$	
201	$+0.0258 - 0.3496i$	$-0.035793677907 - 0.923314870455i$	

into consideration when examining the role of degeneracy [11] or transient growth mechanisms [12] in triggering transition by means of direct Navier–Stokes integration. Numerical technique insensitive (to some extent) to the roundoff errors at a large number of collocation points (Chebyshev polynomials) may be useful in this case.

B. *Navier–Stokes Solver: Accuracy and Stability a priori Estimates*

In the previous section we examined the Navier–Stokes eigenvalue spectrum in order to carry out the preliminary monitoring of the suggested spatial discretization. In particular, it was shown that there are no spurious or parasitic modes among the numerical eigensolutions of the linearized equations.

Nevertheless, additional errors can be introduced both by the time advancing scheme and the solution procedure for the discretized equations. A convenient way (see, e.g., [27]) to check the discrete Navier–Stokes solver accuracy, stability, and sensitivity to the roundoff errors is the evaluation and comparison of the eigenvalues sets $\{\lambda_j(\alpha_m, n, Re)\}$, $\{\bar{\lambda}_j(\alpha_m, n, Re, Q)\}$, and $\{\tilde{\lambda}_j(\alpha_m, n, Re, Q, \Delta t, S)\}$ the last being the spectrum of fully discrete Navier–Stokes equations linearized about their stationary solutions. Nonlinear calculations usually show [7] that *a priori* estimates of accuracy and stability based on the reasonable closeness of the above-mentioned eigensolutions permit us to select adequate values of Q, Δt, S depending on the parameters Re, X, M, N of the mathematical model.

We continue by explaining the technology of $\{\tilde{\lambda}_j\}$ evaluation and by analyzing the results obtained. It can be easily shown that formulas (46) taken at $r = r_l$ determine stationary

TABLE 3
Convergence of the Least Stable Eigenvalue $Re = 4000$, $\alpha_m = n = 20$

Q + 1	re($\bar{\lambda}_1$)	im($\bar{\lambda}_1$)
31	−0.839	−12.642
41	−1.0395775	−1.476281
51	−1.039578126	−1.476280146
61	−1.03957812187	−1.47628014065
71	−1.03957812185209	−1.47628014063815
81	−1.03957812185208327	−1.476280140638094303
91	−1.0395781218520833192	−1.4762801406380943001
101	−1.0395781218520833192	−1.4762801406380943001

TABLE 4
Ten Leading Eigenvalues $\{\bar{\lambda}_k\}_{k=1}^{10}$ Depending on Spatial Resolution; $Re = 4000$, $\alpha_m = n = 20$

	Q + 1 = 41	Q + 1 = 61	Q + 1 = 81	Q + 1 = 101
1	−1.0396 −1.4763*i*	−1.0396 −1.4763*i*	−1.0396 −1.4763*i*	−1.0396 −1.4763*i*
2	−1.1738 −2.3054*i*	−1.1738 −2.3054*i*	−1.1738 −2.3054*i*	−1.1738 −2.3054*i*
3	−1.1764 −14.1882*i*	−1.6561 −2.5602*i*	−1.6561 −2.5602*i*	−1.6561 −2.5602*i*
4	−1.1789 −13.4565*i*	−2.0152 −15.6137*i*	−2.0290 −2.8932*i*	−2.0290 −2.8932*i*
5	−1.1870 −14.8930*i*	−2.0169 −16.0459*i*	−2.1021 −17.8053*i*	−2.1021 −17.8053*i*
6	−1.1933 −12.7022*i*	−2.0216 −15.1640*i*	−2.1310 −3.4569*i*	−2.1310 −3.4569*i*
7	−1.2054 −13.8031*i*	−2.0274 −16.4586*i*	−2.2299 −3.8621*i*	−2.2299 −3.8621*i*
8	−1.2108 −14.5228*i*	−2.0290 −2.8932*i*	−2.2998 −17.6039*i*	−2.2998 −17.6039*i*
9	−1.2126 −13.0588*i*	−2.0356 −14.6982*i*	−2.3038 −17.9873*i*	−2.3038 −17.9873*i*
10	−1.2128 −15.5667*i*	−2.0476 −16.8493*i*	−2.4976 −17.4025*i*	−2.4976 −17.4025*i*

solutions of Eqs. (21). We linearize (21) about these solutions. The result can be written as (the case $n > 0$ for definiteness)

$$\left(\frac{2}{\Delta t} - \nu L^f\right)\overset{(s)}{\mathbf{F}}{}^{k+1}|_l + R^f\,\overset{(s)}{\mathbf{P}}{}^{k+1}|_l = \tau_0^f\delta_{l0} + \tau_Q^f(1-\delta_{n1})\delta_{lQ} + \left(\frac{2}{\Delta t} + \nu L^f\right)\mathbf{F}^k|_l - i\alpha_m U^0(r_l)F_l^k + X^f\mathbf{U}^k|_l - i\alpha_m U^0(r_l)\,\overset{(s-1)}{F}{}_l^{k+1} + X^f\,\overset{(s-1)}{\mathbf{U}}{}^{k+1}|_l, \tag{54a}$$

$$l = 0, 1, \ldots, Q, \qquad \overset{(s)}{F}{}_0^{k+1} = 0, \qquad \overset{(s)}{F}{}_Q^{k+1} = 0\ (n > 1)$$

$$\left(\frac{2}{\Delta t} - \nu L^g\right)\overset{(s)}{\mathbf{G}}{}^{k+1}|_l + R^g\,\overset{(s)}{\mathbf{P}}{}^{k+1}|_l = \tau_0^g\delta_{l0} + \tau_Q^g(1-\delta_{n1}-\delta_{n2}-\delta_{n3})\delta_{lQ} + \left(\frac{2}{\Delta t} + \nu L^g\right)\mathbf{G}^k|_l - i\alpha_m U^0(r_1)G_l^k + X^g\mathbf{U}^k|_l - i\alpha_m U^0(r_l)\,\overset{(s-1)}{G}{}_l^{k+1} + X^g\,\overset{(s-1)}{\mathbf{U}}{}^{k+1}|_l, \tag{54b}$$

$$l = 0, 1, \ldots, Q, \qquad \overset{(s)}{G}{}_0^{k+1} = 0, \qquad \overset{(s)}{G}{}_Q^{k+1} = 0\ (n > 3)$$

$$\left(\frac{2}{\Delta t} - \nu L^u\right)\overset{(s)}{\mathbf{U}}{}^{k+1}|_l + i\alpha_m\,\overset{(s)}{P}{}_l^{k+1} = \tau_0^u\delta_{l0} + \tau_Q^u(1-\delta_{n1})\delta_{lQ} + \left(\frac{2}{\Delta t} + \nu L^u\right)\mathbf{U}^k|_l - i\alpha_m U^0(r_l)U_l^k + r_l^2F_l^k + a_lG_l^k - i\alpha_m U^0(r_l)\,\overset{(s-1)}{U}{}_l^{k+1} + r_l^2\,\overset{(s-1)}{F}{}_l^{k+1} + a_l\,\overset{(s-1)}{G}{}_l^{k+1}, \tag{54c}$$

$$l = 0, 1, \ldots, Q, \qquad \overset{(s)}{U}{}_0^{k+1} = 0, \qquad \overset{(s)}{U}{}_Q^{k+1} = 0\ (n > 1)$$

$$H^f\mathbf{F}^{(s)k+1}|_l + H^g\mathbf{G}^{(s)k+1}|_l + 2i\alpha_m U^{(s)k+1}{}_l = 0, \qquad l = 0, 1, \ldots, Q_f, \qquad P^{(s)k+1}{}_Q = 0 \qquad (n > 1), \tag{54d}$$

where $\nu = 1/Re$; $a_l = 1$ $(n = 1)$, $a_l = r_l^2$ $(n > 1)$; $s = 1, 2, \ldots, S$ is the iteration counter; $\mathbf{F}^k$, $\mathbf{G}^k$, $\mathbf{U}^k$, and $\mathbf{P}^k$ are the Fourier coefficients of disturbances: $\mathbf{F}^k = (F_0^k, F_1^k, \ldots, F_Q^k)^T$, $F_l^k = \tilde{f}_{nm}^F(r_l, t_k)$ and analogously for $\mathbf{G}^k$, $\mathbf{U}^k$, and $\mathbf{P}^k$. Matrices X^f and X^g that appeared at the right hand sides of Eqs. (54) in the course of linearization are defined as

$$X_{lj}^f = B_{lj}(U^0(r_l) - U^0(r_j)) + (n - \sigma_n)S_{lj}(U^0(r_j) - U^0(r_l)) - 2E_{lj},$$

$$X_{lj}^g = \begin{cases} r_l^2 U^0(r_l) B_{lj} - D_{lj} U^0(r_j) - 2r_l^2 E_{lj}, & n = 1, \\ B_{lj}(U^0(r_1) - U^0(r_j)) + (n + \sigma_n)S_{lj}(U^0(r_l) - U^0(r_j)) - 2E_{lj}, & n > 1. \end{cases}$$

Notice that $X^f\mathbf{U}$, $X^g\mathbf{U} \not\equiv 0$ because operators S and B are exact only on the polynomials of degree not higher than $2Q$.

The resolve Eqs. (54) (that is, to express the unknown quantities relating to $t = t_{k+1}$ and iteration loop s through the ones at $t = t_k$ and preceding iteration) we exploit the numerical method of Sections V, VII. Limiting ourselves to $\alpha_m \neq 0$ and dropping intermediate calculations we obtain then

$$\overset{(s)}{\mathbf{x}}{}^{k+1} = T_1\mathbf{x}^k + T_2\,\overset{(s-1)}{\mathbf{x}}{}^{k+1},\ s \geq 1, \qquad \mathbf{x} = (F_1, F_2, \ldots, F_{Q_f}, G_1, G_2, \ldots, G_{Q_g})^T, \quad (55)$$

where complex $(Q_f + Q_g) \times (Q_f + Q_g)$ matrices T_1, T_2 are functions of α_m, n, Re, Q, and Δt. By evaluating initial approximations as

$$\overset{(0)}{\mathbf{x}}{}^{k+1} = 2\mathbf{x}^k - \mathbf{x}^{k-1},$$

we obtain from recurrence relations (55)

$$\overset{(S)}{\mathbf{x}}{}^{k+1} = T_3\mathbf{x}^k - T_2^S\mathbf{x}^{k-1}, \quad (56)$$

where

$$T_3 = 2T_2^S + \left(T_2^{S-1} + T_2^{S-2} + \cdots + T_2 + E\right)T_1.$$

Matrices T_3 and T_2 do not depend on index k. Therefore we seek solutions of Eqs. (56) in the form

$$\overset{(S)}{\mathbf{x}}{}^{k+1} = \overset{(S)}{\rho}{}^{k+1}\mathbf{x},$$

where $\overset{(S)}{\rho}$ and $\mathbf{x}$ are among the eigensolutions of the spectral problem

$$\overset{(S)}{\rho}\mathbf{y} = T\mathbf{y} = \begin{pmatrix} T_3 & -T_2^S \\ E & 0 \end{pmatrix}\mathbf{y}, \qquad \mathbf{y} = (\overset{(S)}{\rho}\mathbf{x}, \mathbf{x})^T. \quad (57)$$

Desired eigenvalues $\tilde{\lambda}_j = \tilde{\lambda}_j(\alpha_m, n, Re, Q, \Delta t, S)$ are evaluated then by the formulas

$$\tilde{\lambda}_j = \frac{1}{\Delta t}\ln\overset{(S)}{\rho}_j, \qquad j = 1, 2, \ldots, Q_f + Q_g. \quad (58)$$

Comparison of the fully discrete eigenvalues $\{\tilde{\lambda}_j\}$ with $\{\bar{\lambda}_j\}$ and $\{\lambda_j\}$, $re\lambda_j \geq re\lambda_{j+1}$ allows one to make certain conclusions concerning stability and accuracy characteristics of

TABLE 5

Eigensolutions of the Discrete and Differential Spectral Problems; $Re = 4000$, $S = 2$

α_m, n	Δt	$\bar{\lambda}_1(\alpha_m, n, Re, Q, \Delta t, S)$						$\bar{\lambda}_1(\alpha_m, n, Re, Q), \lambda_1(\alpha_m, n, Re)$
		Q = 30		Q = 40		Q = 50		
1, 1	0.8	−0.0405	−3.93i	−0.0129	−3.93i	−0.00527	−3.93i	$\bar{\lambda}_1 = -0.0358 - 0.923i$ (Q = 30)
	0.4	−0.0462	−0.916i	−0.0462	−0.916i	−0.0211	−7.85i	$\lambda_1 = -0.0358 - 0.923i$
	0.2	−0.0370	−0.921i	−0.0370	−0.921i	−0.0370	−0.921i	
	0.1	−0.0359	−0.923i	−0.0359	−0.923i	−0.0359	−0.923i	
	0.05	−0.0358	−0.923i	−0.0358	−0.923i	−0.0358	−0.923i	
10, 10	0.2	+4.14	−12.4i	+4.14	−12.2i	+4.14	−12.2i	$\bar{\lambda}_1 = -0.512 - 7.70i$ (Q = 30)
	0.1	−0.474	−5.11i	−0.573	−0.928i	−0.337	+31.4i	$\bar{\lambda}_1 = -0.574 - 0.928i$ (Q = 40)
	0.05	−0.317	−6.68i	−0.574	−0.928i	−0.574	−0.928i	$\lambda_1 = -0.574 - 0.928i$
	10^{-3}	−0.262	−7.21i	−0.574	−0.928i	−0.574	−0.928i	
	10^{-4}	−0.262	−7.21i	−0.574	−0.928i	−0.574	−0.928i	
20, 20	0.1	+7.59	−24.5i	+7.47	−24.4i	+7.46	−24.4i	$\bar{\lambda}_1 = -0.839 - 12.6i$ (Q = 30)
	0.05	−0.651	−8.24i	−1.04	−1.48i	−1.04	−1.48i	$\bar{\lambda}_1 = -1.04 - 1.48i$ (Q = 40)
	0.025	−0.477	−11.4i	−0.919	−12.5i	−1.04	−1.48i	$\lambda_1 = -1.04 - 1.48i$
	0.0125	−0.429	−11.5i	−0.849	−13.3i	−1.04	−1.48i	
	10^{-3}	−0.421	−12.5i	−0.840	−13.4i	−1.04	−1.48i	
	10^{-4}	−0.421	−12.5i	−0.840	−13.4i	−1.04	−1.48i	
42, 42	0.05	+14.7	−49.6i	+14.4	−49.5i	+14.2	−49.5i	$\bar{\lambda}_1 = -1.92 - 18.2i$ (Q = 30)
	0.025	−1.59	−13.3i	−2.19	−16.6i	−2.27	−2.42i	$\bar{\lambda}_1 = -2.27 - 2.42i$ (Q = 40)
	10^{-3}	−1.42	−17.7i	−1.88	−21.7i	−2.27	−2.42i	$\lambda_1 = -2.27 - 2.42i$
	10^{-4}	−1.42	−17.7i	−1.88	−21.7i	−2.27	−2.42i	

the numerical method as well as to make the preliminary selection of its parameters. For example, in Table 5 we compare the least stable discrete eigenvalues $\tilde{\lambda}_1$ evaluated by means of algorithm (54)–(58) with the corresponding eigenvalues of the differential problem.

It should be stressed in addition, that the procedure of matrix T evaluation is just the same as suggested in Sections V and VII. Therefore, computations by means of formulas (54)–(58) may indicate the effect of computer roundoff errors.

Such information cannot be obtained by means of a popular method based on the stability region concept [23]. The latter technique can be exploited only when the same time integration scheme is used both for viscous and convective terms. For example, with the implicit Crank–Nicolson method Eqs. (55) take the form

$$(\mathbf{x}^{k+1} - \mathbf{x}^k)/\Delta t = \bar{T}(\mathbf{x}^{k+1} + \mathbf{x}^k)/2, \tag{59a}$$

and with certain predictor-corrector method

$$\left({}^{(s)}\mathbf{x}^{k+1} - \mathbf{x}^k\right)/\Delta t = \bar{T}\left({}^{(s-1)}\mathbf{x}^{k+1} + \mathbf{x}^k\right)/2 \ (s = 1, 2, \ldots, S), \qquad {}^{(0)}\mathbf{x}^{k+1} = 2\mathbf{x}^k - \mathbf{x}^{k-1}, \tag{59b}$$

where $\bar{T}$ is the matrix from Eq. (48). In both cases each eigenvalue ρ of the conversion matrix from time step t_k to time step t_{k+1} is defined by the product of Δt times the corresponding eigenvalue $\bar{\lambda}(\alpha_m, n, Re, Q)$ of matrix $\bar{T}$,

$$\rho = \left(1 + \frac{1}{2}\bar{\lambda}\Delta t\right) \Big/ \left(1 - \frac{1}{2}\bar{\lambda}\Delta t\right), \tag{60a}$$

for (59a) and

$$\overset{(S)}{\rho}{}^2 - \overset{(S)}{\rho}\left(1 + \bar{\lambda}\Delta t\frac{1-(0.5\bar{\lambda}\Delta t)^S}{1-0.5\bar{\lambda}\Delta t} + (0.5\bar{\lambda}\Delta t)^S\right) + (0.5\bar{\lambda}\Delta t)^S = 0, \qquad (60b)$$

for (59b). And what is more, formulas (59), (60) differ from the actual solution procedure for the discrete Navier–Stokes equations. Therefore, the concept of stability regions on the complex plane $\bar{\lambda}\Delta t$ cannot be used to examine the effect of roundoff errors on the accuracy and sometimes even on the stability limit of computations.

C. *Direct Navier–Stokes Simulation of Laminar-Turbulent Transition at Re* $= 4000$

Initial disturbances of laminar pipe Poiseuille flow were specified using superposition of axisymmetric and nonaxisymmetric eigenfunctions of the Navier–Stokes equations linearized about the parabolic velocity profile. Concretely, we used three least stable vector eigenfunctions corresponding to Fourier modes with wavenumbers $(\alpha_m, n) = (1, 0); (0, 1); (1, 1)$ and energies

$$E_{nm} = \frac{1}{\pi R^2 X}\int_{\mathcal{G}} d\mathbf{r}\frac{\mathbf{v}_{nm}^2}{2} = 10^{-3}$$

each. Time evolution of these finite-amplitude disturbances was calculated until the statistically stationary turbulent flow regime was established. Computations were carried out with $(Q+1)\times(2N+1)\times(2M+1) = 33\times 41\times 41$ basis functions in r, φ, x at $Re = 4000 (Re_{CL} = \bar{u}_{CL} D/\nu \approx 5432, Re_\tau = u_\tau D/\nu \approx 289)$ and $X = \pi D (X^+ = X u_\tau/\nu \approx 907)$. Here $\bar{u}_{CL}$ and u_τ are the mean centreline and wall-shear velocities. Minimum and maximum grid spacings in r are 0.17 (the first mesh point away from the wall) and 7.09 in wall units. The minimal resolved wavelengths in φ (at $r = R$, along the pipe surface) and x are $\lambda_\varphi = \pi D/N \approx 45.36\nu/u_\tau$ and $\lambda_x = X/M \approx 45.36\nu/u_\tau$.

The computed time history of laminar-turbulent transition is shown in Figs. 1, 2. The primary stabilization of basic integral flow characteristics such as the space-averaged pressure gradient and kinetic energy of disturbances (Fig. 1(a)) as well as of the mean (φ and x-averaged) velocity profile (Fig. 2(a)) is rather a rapid process taking of about 100 nondimensional time units (4000 time steps). It should be noted that time interval $t \in [50, 100]$ often proves to be the bane of numerical simulation, due to very rapid reorganization of the flow field at the late stage of transition and the strongly nonlinear nature of this process. We remind also that our computations were carried out under the condition of volume flux constancy (see Fig. 1(b) and Eq. (3c)). Otherwise (e.g., if the space-averaged pressure gradient is assumed to be fixed), duration of the transient regime may be several times longer. The total integration time was about $T \approx 1500$ (see Fig. 1(a)) with the averaging time $\bar{T} \approx 500 \approx 18R/u_\tau \approx 2659\nu/u_\tau^2$ ($t \in [1000, 1500]$, Fig. 1(a)) and computational time step $\Delta t = 0.025 \approx 9.03\times 10^{-4} R/u_\tau \approx 0.13\nu/u_\tau^2$.

The mean velocity profiles as well as the computed Reynolds shear stress are compared with those of experimental and numerical data [28, 29, 3] in Figs. 2(b), 4(a). Here and below the computed mean and r.m.s. values are φ, x, and time-averages. The agreement is quite satisfactory in spite of the fact that present spectral calculations are carried out with much less number of basis functions compared with the number of grid points exploited by the finite-difference scheme of [3]. Note also, that the congruence of the computed

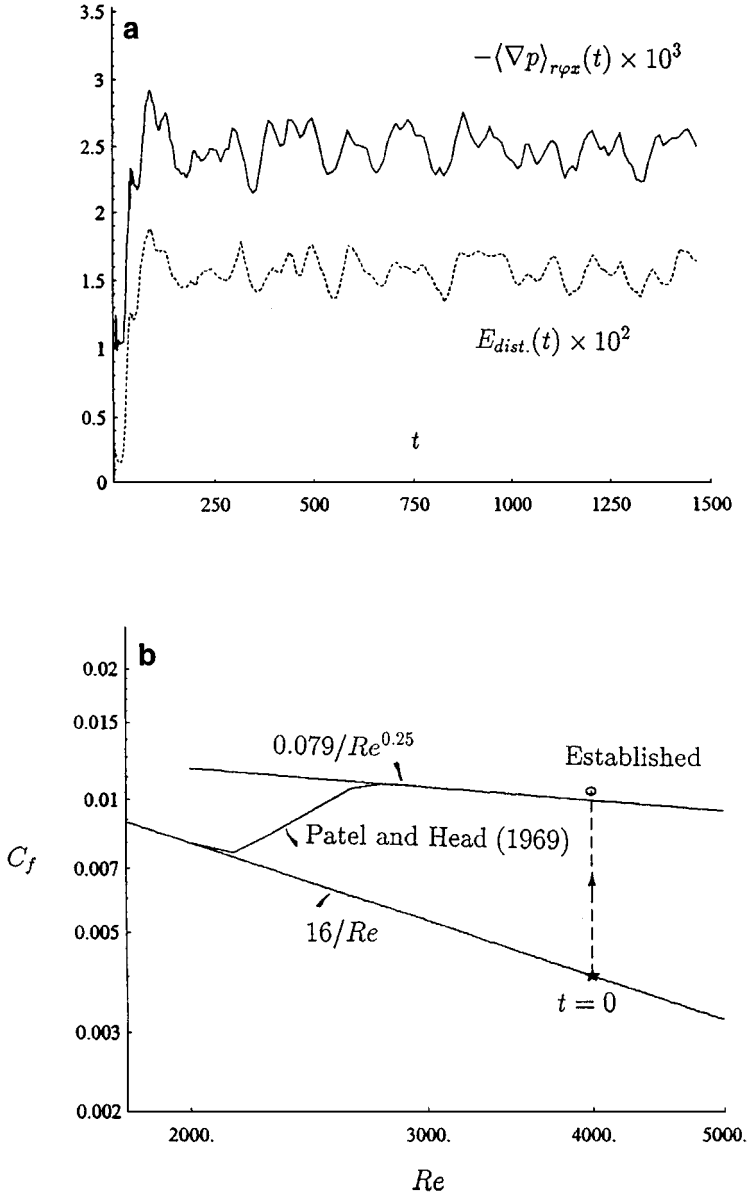

FIG. 1. (a) Time history of the laminar-turbulent transition in a circular pipe under the condition of flow flux constancy; $\langle\nabla p\rangle_{r,\varphi,x}$ is the non-dimensionalized space-averaged pressure gradient (initial value of -10^{-3} corresponds to laminar pipe flow pressure gradient $-4/Re$), E_{dist} is the total kinetic energy of disturbances. (b) Skin-friction coefficient $C_f = -\langle\nabla p\rangle_{r,\varphi,x,t} D/2\rho\bar{U}^2$ versus Reynolds number. An arrow connects initial and final states of the transition process: point "$\star$" corresponds to the disturbed laminar flow (initial condition of our Navier–Stokes simulation), and point "$\circ$" to the established turbulent flow regime. Intermediate stages of transition all correspond to arrow points between $\star$ and $\circ$. The computed turbulent value of $C_f \approx 1.04 \times 10^{-2}$ (point $\circ$) agrees well with Blasius friction law $C_f = 0.079Re^{-1/4} \approx 9.93 \times 10^{-3}$ (about 5% difference) at $Re = 4000$.

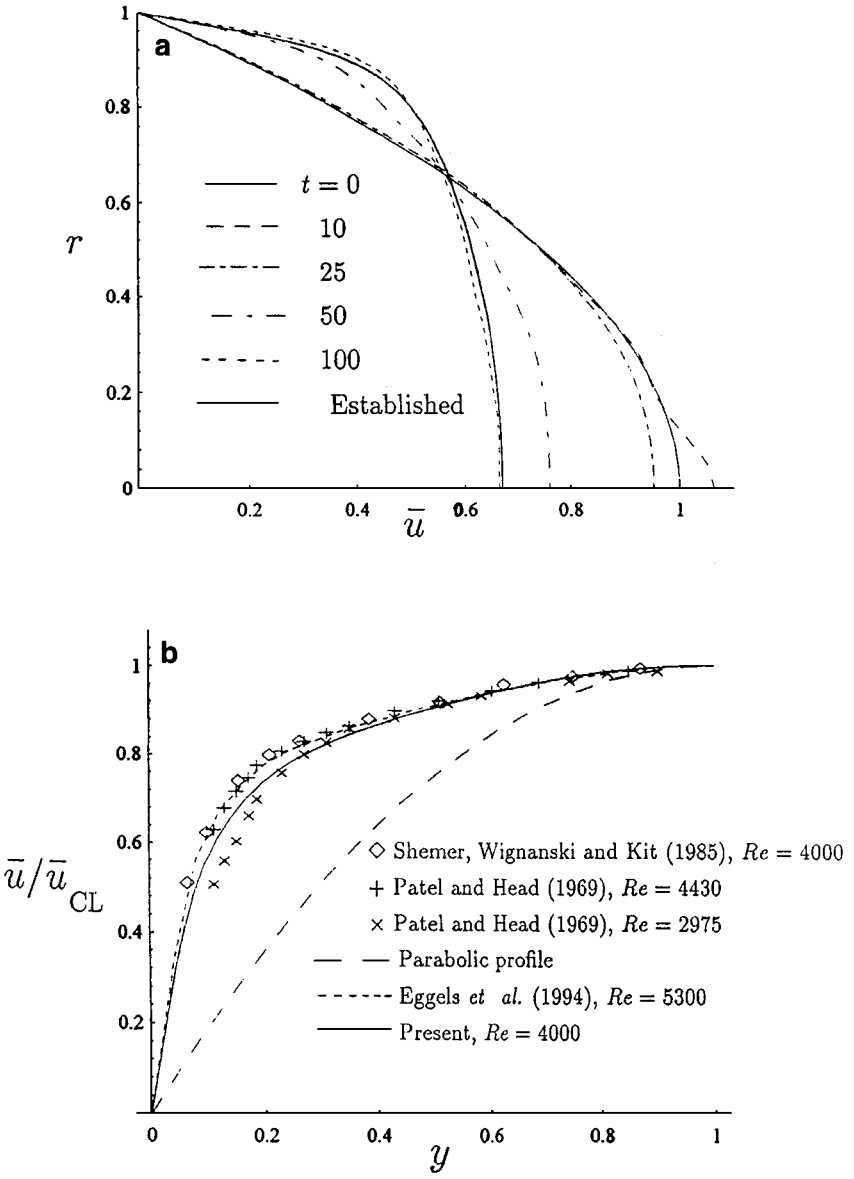

FIG. 2. (a) Mean velocity profiles in the course of laminar-turbulent transition in a circular pipe at $Re = 4000$. (b) Mean velocity profiles normalized by the centreline velocity ($y = 1 - r/R$).

total shear stress with the straight line indicates both that the statistical sample is adequate and that the computed results correspond to the equilibrium state. Analogous conclusions can be made by examining Fig. 3 where the r.m.s. velocity fluctuations are presented. The distributions of root-mean-square vorticity fluctuations are shown in Fig. 4(b). In Fig. 5 we compare them in the near-wall region with those of high resolution channel flow simulations [30].

As far as we know this is the first direct simulation of all stages of laminar-turbulent transition in a circular pipe. Previous investigations dealt with either established turbulent pipe flows [2, 3, 8] or initial stages of transition [6]. Thus, the algorithm presented seems to be

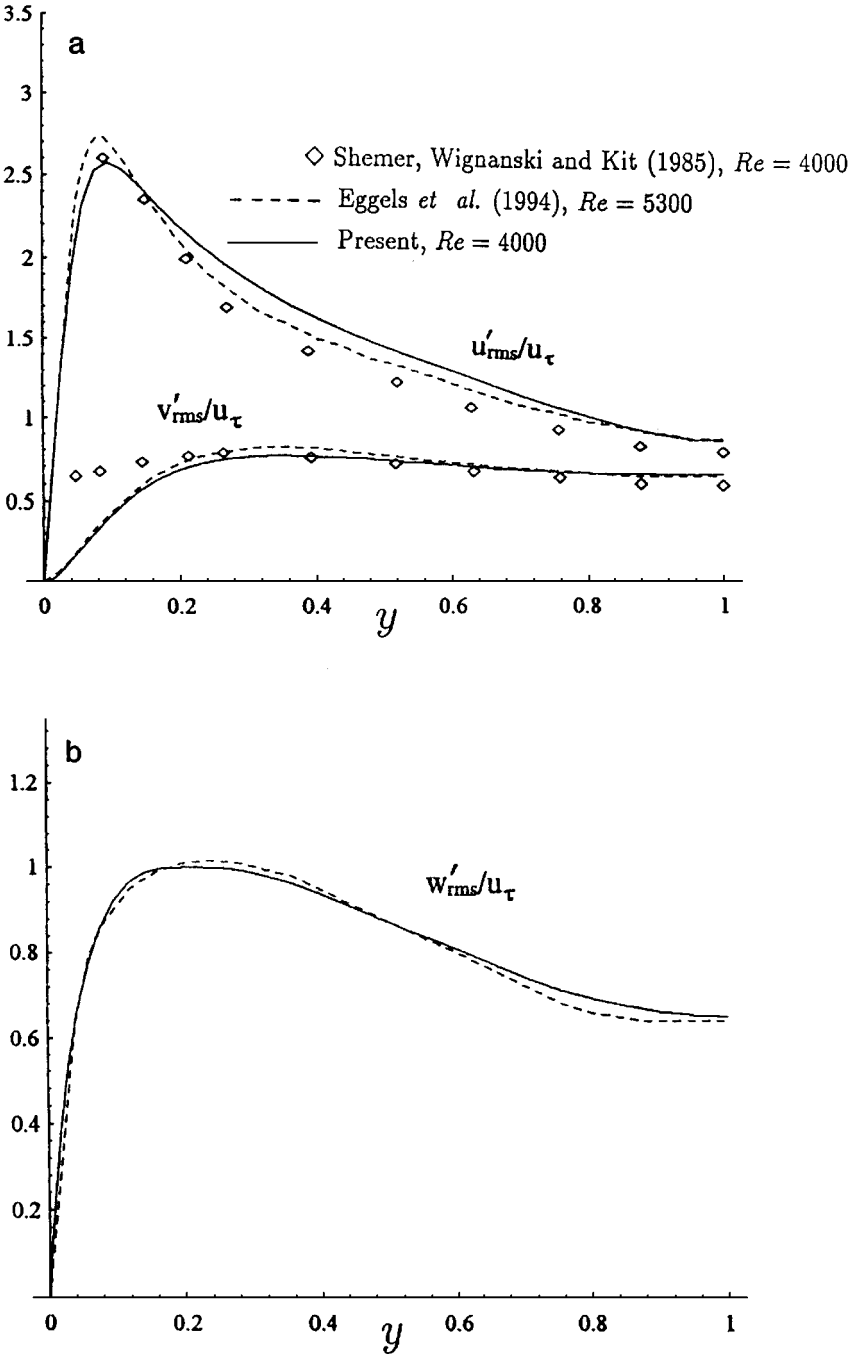

FIG. 3. Root-mean-square velocity fluctuations as functions of distance $y = 1 - r/R$ from the pipe wall: (a) streamwise and radial; (b) azimuthal velocity components.

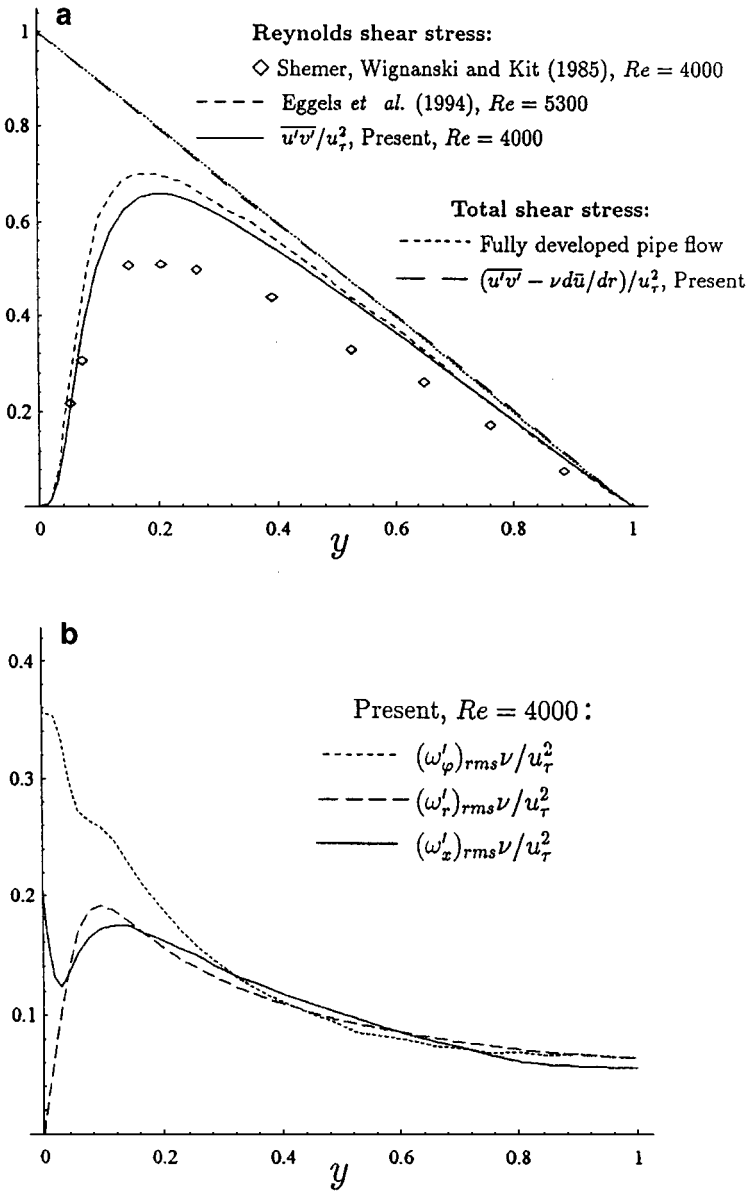

FIG. 4. (a) Reynolds and total shear stress distributions. (b) Root-mean-square vorticity fluctuations in global coordinates.

a ready-to-use robust tool for accurate numerical simulation and future well-resolved parametric studies of both transition mechanisms and fully developed turbulent flow regimes.

IX. DISCUSSION

Up to this point, when searching for the numerical Navier–Stokes solutions in the form (10), we did not presuppose the existence of any symmetry restrictions. Meanwhile, similar hypotheses are often made in the course of boundary layer and channel flow simulations when the flow field is assumed to be symmetric with respect to the plane $z = 0$, z being the

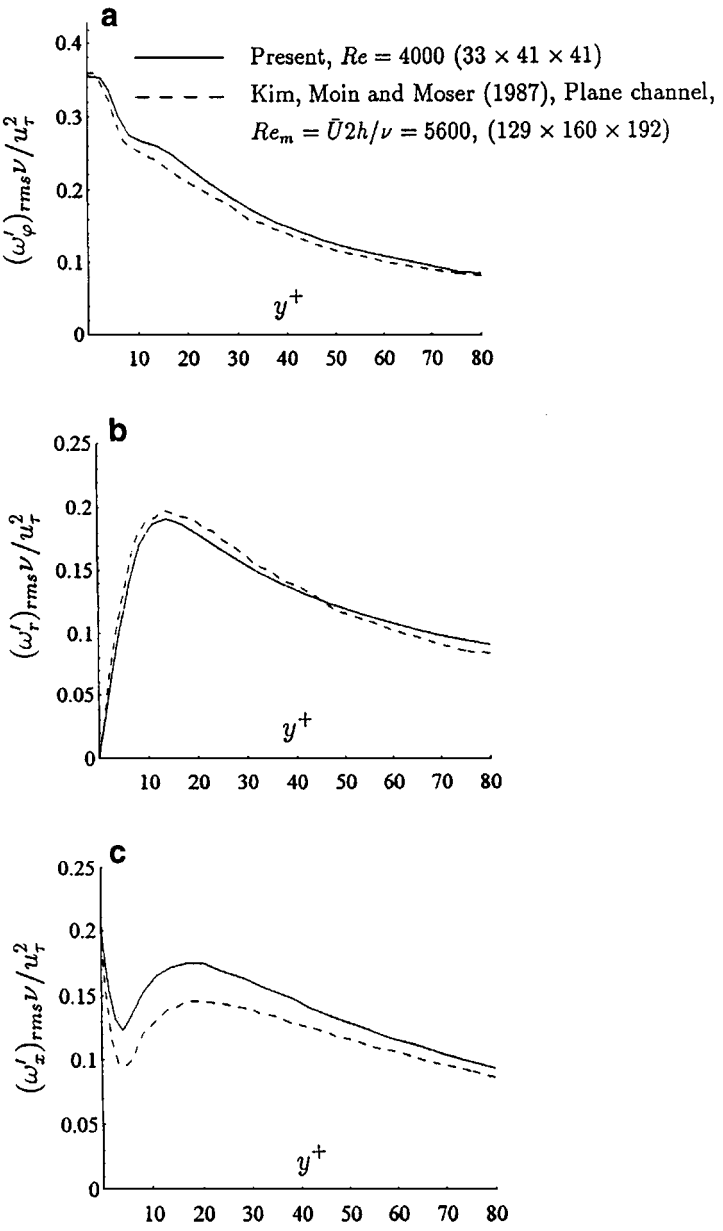

FIG. 5. Root-mean-square vorticity fluctuations in the near wall region.

spanwise coordinate (see, e.g., [31–33]). In Cartesian coordinates the spanwise-symmetric Navier–Stokes solutions seem to be adequate: comparison of the computed turbulent flow characteristics with those obtained in the laboratory gives satisfactory results. Nevertheless, until now no serious theoretical arguments are shown on behalf of the possibility to describe transitional and turbulent flow regimes by means of spanwise-symmetric (at every moment of time!) Navier–Stokes solutions. Possibly, this is the reason why in the most thorough and accurate calculations (see, e.g., [30]) numerical solutions are not assumed *a priori* to have certain symmetries.

In cylindrical coordinates the "spanwise" symmetry of the velocity field means that

$$\begin{aligned} v(r,\varphi,x,t) &= v(r,-\varphi,x,t),\\ w(r,\varphi,x,t) &= -w(r,-\varphi,x,t),\\ u(r,\varphi,x,t) &= u(r,-\varphi,x,t), \end{aligned} \tag{61}$$

and these relations are formally preserved by the Navier–Stokes equations (2a), (2b) and boundary conditions (2c), (3). From the computational point of view it is rather tempting to assume that turbulent flow may have such a symmetry. Indeed, in this case one can exploit the sparse set of Fourier modes instead of general representation (10). As it follows from Eqs. (29) and (61)

$$v_n^S(r,x,t) \equiv 0, \qquad w_n^C(r,x,t) \equiv 0, \qquad u_n^S(r,x,t) \equiv 0, \tag{62}$$

so that the computational complexity of simulation may be considerably reduced. See, e.g., [34] where symmetry restrictions (61) are exploited for the turbulent pipe flow simulation.

However, in contrast to Cartesian coordinates we can produce certain reasons justifying the inability of the Navier–Stokes solutions (61) to describe actual turbulent flow in $\mathcal{G}$. In fact, if Eqs. (62) are correct, we obtain instead of (38)

$$\omega_x(r,\varphi,x,t) = r(\bar{\omega}_x)_1^S \sin\varphi + r^2 \sum_{n=2}^{N} r^{\sigma_n} (\bar{\omega}_x)_n^S \sin n\varphi, \tag{63}$$

where functions $(\bar{\omega}_x)_n^S$ are defined by Eqs. (39) as before. We remind that formulas (63) follow directly from Theorem 1 that governs the asymptotic behaviour of analytic functions at $r \to 0$. Note that as it follows from Eqs. (63), the instantaneous values as well as the root-mean-square fluctuations of the streamwise vorticity become zero at the polar axis.

The latter property contradicts certain known computational results for the turbulent flow vorticity values far away from channel or pipe walls. Indeed, in channel flow calculations [30, Fig. 14(a)] all three components of the fluctuating vorticity have almost equal nonzero values at the channel centerline. An analogous result is obtained in the present paper (Fig. 4(b)) for general Navier–Stokes solutions having no symmetry restrictions. In addition, such a behaviour of vorticity components looks very plausible from the physical point of view. As to the existing experimental data on vorticity fluctuations, it seems to be limited to the near-wall region and therefore cannot be used to determine if the Navier–Stokes solutions (61) can describe any turbulent flow regimes.

To clarify the issue, i.e., to understand if the approximate Navier–Stokes solutions (61) really exist and what is their relationship with actual turbulent flows in $\mathcal{G}$, we have carried out a special investigation. The latter involved both the description of laminar-turbulent transition and the evaluation of those turbulent flow characteristics that correspond to well established experimental data.

As a result we can conclude that the use of symmetry relations (61) in the course of numerical simulation turns out to be rather insidious. First of all, the numerical Navier–Stokes solutions (61) do exist: pipe Poiseuille flow is unstable with respect to finite amplitude azimuthally symmetric disturbances and statistically steady ("turbulent") solutions can be really computed. Second, certain basic turbulence characteristics are almost insensitive (e.g., the skin-friction coefficient as well as the root-mean-square fluctuations of streamwise and radial velocity components shown in Fig. 7(a)) or weakly sensitive (the Reynolds shear stress, Fig. 8(a)) to the incorporating of symmetry relations into the numerical model.

However, there exist such well-established flow characteristics that cannot be adequately described by the azimuthally symmetric solutions. Among them are the mean velocity profile and r.m.s. fluctuations of the azimuthal component of velocity (Figs. 6, 7(b)). But the most striking disagreement between azimuthally symmetric and general form solutions represents the streamwise component of vorticity (compare Figs. 4(b) and 8(b)). Thus, in contrast to the plane channel and boundary layer flows, the "spanwise" (azimuthally) symmetric Navier–Stokes solutions fail to describe some of the basic turbulent flow characteristics in $\mathcal{G}$. It should be noted in conclusion, that we did not examine here the stability of solutions (61) with respect to disturbances of a general form.

One more symmetry group allowed by the Navier–Stokes equations and boundary conditions (2), (3) is defined by the solutions (10) with

$$\mathbf{v}_{2k,2l+1}(r, \varphi, x, t) = 0, \qquad \mathbf{v}_{2k+1,2l}(r, \varphi, x, t) = 0, \qquad k = 0, 1, \ldots, \qquad l = 0, 1, \ldots. \tag{64}$$

Nonstationary Navier–Stokes solutions with symmetry restrictions (64) were computed (among others) using one of the previous versions of our numerical method (algorithm *A*, [7]). These long-life (i.e., undamped at least for about $\Delta T \simeq O(Re)$) solutions describe statistically steady flow regimes in $\mathcal{G}$ with the same skin-friction coefficient, averaged pressure gradient, and kinetic energy of velocity fluctuations as in the case of general Navier–Stokes solutions without any symmetry restrictions. The detailed comparison of turbulence statistics computed by means of symmetric and general solutions was not conducted.

Notice also the following computational peculiarity of the symmetry conditions (64). If we take the velocity field satisfying Eqs. (64) as an initial condition for the Navier–Stokes integration in time, we may reproduce these symmetry relations for arbitrary time even when we use an universal computer code. We may even not suspect that one half

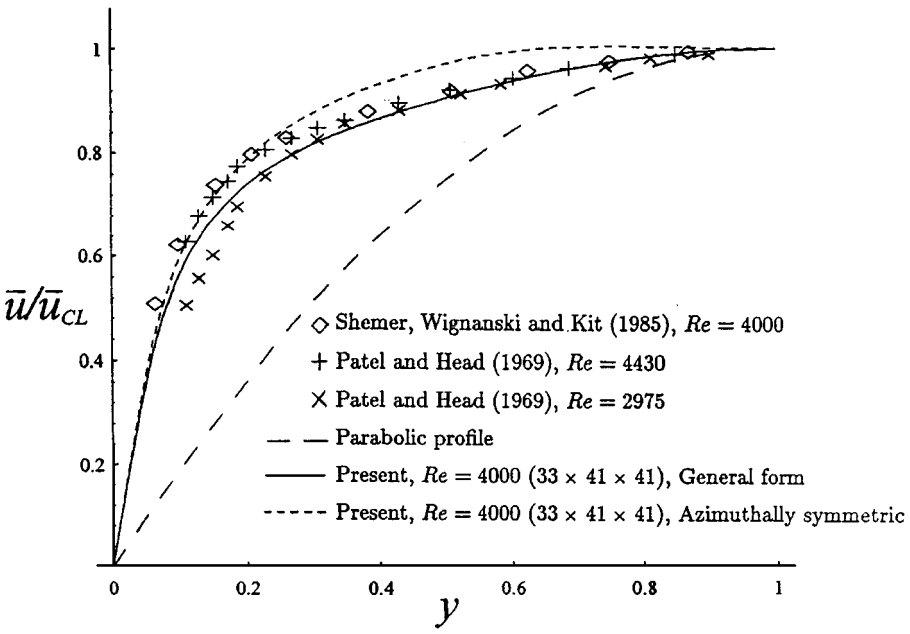

FIG. 6. Mean velocity profiles corresponding to Navier–Stokes solutions of general and azimuthally symmetric forms.

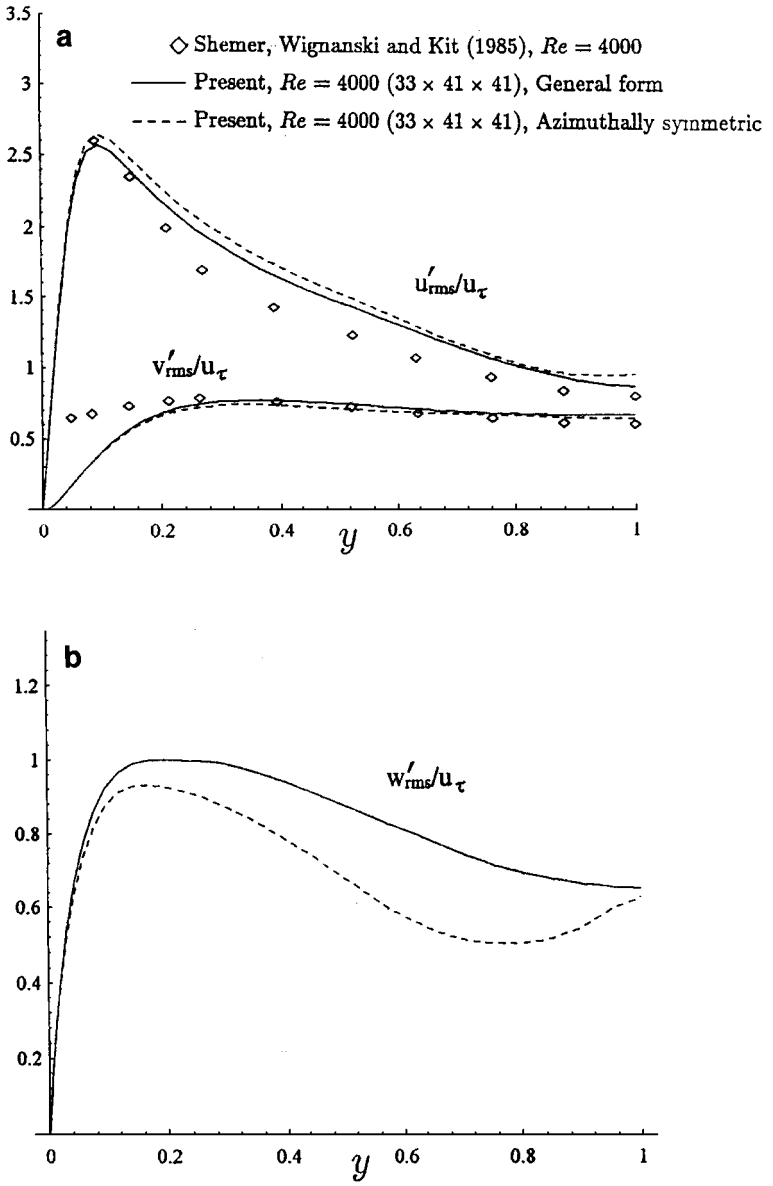

FIG. 7. Comparison of the r.m.s. velocity distributions corresponding to Navier–Stokes solutions of general and azimuthally symmetric forms.

of our Fourier modes remains equal to zero in the course of calculation. For example, if our initial condition is the superposition of the base parabolic flow and any eigensolution corresponding to wavenumbers $(m, n) = (1, 1)$ we'll be able to compute only solutions belonging to the class of functions (64). Roundoff errors may not play the usual destabilizing role here because the result of the multiplication of a nonzero value by the machine zero is often interpreted as the zero constant by the computer. That is just the case when we compute the quadratic nonlinear terms of the Navier–Stokes equations.

Of course, the foregoing investigation of some symmetry relations and their suitability for the Navier–Stokes turbulent flow simulation is incomplete. Additional examples

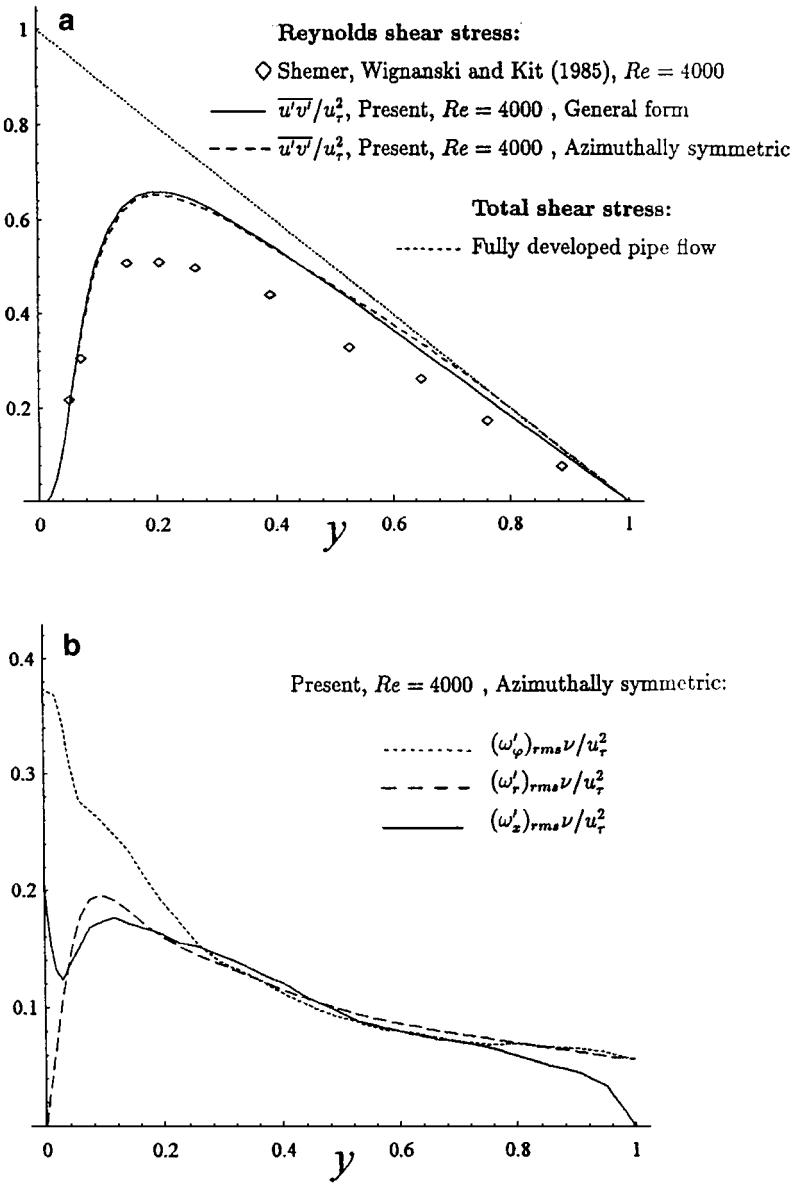

FIG. 8. Comparison of the Reynolds shear stress distributions (a) and r.m.s. vorticity fluctuations (b) corresponding to Navier–Stokes solutions of general and azimuthally symmetric forms.

of symmetries allowed by the incompressible Navier–Stokes equations can be found in [35, 36] concerned with Taylor–Couette and spherical Couette flows. In the present investigation we intended to show possible difficulties as well as the existence of certain solutions in principle. Is there any relation between symmetry and some special physics? Are symmetric solutions stable with respect to disturbances of general form? Are there any simplifications of the space-time structure of velocity and pressure fields described by the symmetric solutions compared with those of general form? Are symmetric solutions approaching those of general form in the limit when the Reynolds number is very large?

These problems require additional thorough investigation. We hope that our accurate and fast numerical method can be exploited for that purpose.

X. SUMMARY AND CONCLUSIONS

We have presented a fast, accurate, and robust pseudospectral Navier–Stokes algorithm suitable for numerical investigation of laminar, transitional, and turbulent incompressible fluid flow regimes in a circular pipe. Moreover, a new algorithm (or its fragments) may have wider applicability including the situations when computational domain contains coordinate singularity along the polar axis $r = 0$ and when the dependence on azimuth angle φ can be represented as a Fourier series due to physical symmetry of the problem.

The algorithm is based on a new change of dependent variables that avoids singularity problems taking into account special behaviour of analytic functions in the vicinity of a singularity point (Theorem 1). Being written in new variables Navier–Stokes equations can be discretized then without loss of accuracy by using the Galerkin trigonometric approximation in azimuthal and streamwise directions and the Chebyshev collocation technique in r. The use of half Chebyshev grid points with prescribed conditions at $r = 0$ turned out to be justified: spectral (faster than algebraic) convergence of numerical Navier–Stokes solutions in the pipe was achieved. The possible reason for spectral convergence is that the Navier–Stokes solutions obtained proved to be analytic functions in the vicinity of polar axis. In this case their Fourier coefficients may be smoothly extended to the functions on the interval $[-R, R]$. Thus, depending on the azimuth wavenumber the even or odd Chebyshev polynomials become appropriate expansion functions ensuring spectral accuracy.

For integration in time we exploit the Crank–Nicolson method with viscous terms, the backward Euler with the pressure, and the second order predictor-corrector scheme with the nonlinearity. For the solution of resulting discrete Navier–Stokes equations we suggest an efficient and weakly roundoff-sensitive method (Theorem 2). This method is based on the influence matrix technique but has certain modifications (due to the cylindrical geometry and coordinate singularities at $r = 0$).

Another key point of our algorithm is a fast technique for the evaluation of Navier–Stokes nonlinear terms. Direct implementation of the usual pseudospectral method proves to be impossible due to a rather complicated form of nonlinearity written in terms of new variables.

A new algorithm was thoroughly tested: eigensolutions of the pipe Poiseuille flow linear stability problem as well as the total time history of laminar-turbulent transition including the established turbulent flow regime were computed at the supercritical Reynolds number of 4000. In spite of the presence of coordinate singularities the algorithm provides spectral accuracy and is weakly sensitive to the roundoff errors. We stress that the new algorithm allows us to compute all the stages of laminar-turbulent transition in $\mathcal{G}$ in the framework of one mathematical model without tuning its parameters in the course of computations. The latter seems to be very important for future high resolution parametric studies of transition mechanisms and comparisons with corresponding experimental data. Notice also, that our calculations are completely reproducible: in addition to necessary formulas we show the structure and amplitudes of initial disturbances of parabolic base flow (being the eigenvectors of linear stability problem) that finally lead to laminar-turbulent transition.

In conclusion we want to draw attention to the results concerning the existence and usefulness of numerical Navier–Stokes solutions having certain symmetries. In particular,

we managed to show that, in contrast to turbulent channel and flat plate boundary layer flows, the pipe flow turbulence cannot be adequately described by the so-called spanwise-symmetric Navier–Stokes solutions. It should be noted that spanwise symmetry of solutions does not represent some kind of exotic symmetry group: the time averaged Navier–Stokes solutions of general form seem to have such symmetry.

APPENDIX A: MATRIX ELEMENTS OF EQS. (19)

For arbitrary $l, j = 0, 1, \ldots, Q$,

$$C_{lj} = \frac{16\varrho_j}{Q} \sum_{q=0}^{Q} \varrho_q T_{2q}(r_j/R) q \sum_{m=0}^{q} (q-m)(q+m) \frac{T_{2m}(r_l/R)}{c_m},$$

$$B_{lj} = \frac{8\varrho_j}{Q} \sum_{q=0}^{Q} \varrho_q T_{2q}(r_j/R) q \sum_{m=0}^{q} [1-(-1)^{q-m}] \frac{T_{2m}(r_l/R)}{c_m},$$

$$D_{lj} = \frac{8\varrho_j}{Q} \sum_{q=0}^{Q} \varrho_q T_{2q}(r_j/R) q \sum_{m=0}^{q} \rho_m^{(q)} T_{2m}(r_l/R),$$

$$S_{lj} = \frac{8\varrho_j}{Q} \sum_{q=0}^{Q} \varrho_q T_{2q}(r_j/R)(-1)^{q-1} \sum_{m=0}^{q} (q-m)(-1)^m \frac{T_{2m}(r_l/R)}{c_m},$$

where

$$c_0 = 2, \qquad c_m = 1 \ (m \geq 1),$$

$$\varrho_0 = \varrho_Q = 0.5, \qquad \varrho_q = 1 \ (q \neq 0, Q),$$

$$T_{2q}(r_j/R) = \cos\frac{\pi j q}{Q}, \qquad T_{2m}(r_l/R) = \cos\frac{\pi l m}{Q},$$

$$\rho_0^{(q)} = \rho_q^{(q)} = 0.5, \qquad \rho_m^{(q)} = 1 \ (m = 1, 2, \ldots, q-1).$$

APPENDIX B: ADDITIONAL FORMULAS FOR ZERO WAVENUMBERS

1. *Equations* (21) *for* $\alpha_m > 0, n = 0$

Instead of (21) we have

$$\left(\frac{2}{\Delta t}E - \nu L^v\right)\mathbf{V}|_l + B\mathbf{P}|_l = \tau_0^v \delta_{l0} + a_l^v, \qquad l = 0, 1, \ldots, Q,$$
$$V_0 = 0 \tag{21′a}$$

$$\left(\frac{2}{\Delta t}E - \nu L^w\right)\mathbf{W}|_l = a_l^w, \qquad l = 1, 2, \ldots, Q,$$
$$W_0 = 0 \tag{21′b}$$

$$\left(\frac{2}{\Delta t}E - \nu L^u\right)\mathbf{U}|_l + \frac{\partial}{\partial x}P_l = \tau_0^u \delta_{l0} + a_l^u, \qquad l = 0, 1, \ldots, Q,$$
$$U_0 = 0 \tag{21′c}$$

$$(D + 2E)\mathbf{V}|_l + \frac{\partial}{\partial x} U_l = 0, \qquad l = 0, 1, \ldots, Q. \tag{21′d}$$

Here $\mathbf{P} \stackrel{\text{def}}{=} (P_0, P_1, \ldots, P_Q)^T$, $P_j(x) = 2\ \overset{(s)}{\tilde{p}}{}^{k+1}_{0mj} = 2\ \overset{(s)}{\tilde{p}}{}^{k+1}_{0m}|_{r=r_j}$; $\mathbf{V} \stackrel{\text{def}}{=} (V_0, V_1, \ldots, V_Q)^T$, $V_j(x) = \overset{(s)}{\tilde{v}}{}^{k+1}_{0mj}$, analogously for $\mathbf{W}$ and $\mathbf{U}$. Matrices $L^{v,w,u}$ are defined by

$$L^v = L^w = C + 3B - \alpha_m^2 E, \qquad L^u = C + B - \alpha_m^2 E. \tag{23′}$$

2. *Equations* (21) *for* $\alpha_m = 0, n > 0$

Formally, Eqs. (21), (22) may be used in this case. However, we can improve the stability characteristics of the scheme rewriting (21), (22) as

$$\left(\frac{2}{\Delta t} E - \nu L^f\right)\mathbf{F}|_l + R^f \mathbf{P}|_l = \tau_0^f \delta_{l0} + \tau_Q^f (1 - \delta_{n1})\delta_{lQ} + a_l^f, \tag{21″a}$$

$$l = 0, 1, \ldots, Q, \qquad F_0 = 0, \qquad F_Q = 0\ (n > 1)$$

$$\left(\frac{2}{\Delta t} E - \nu L^g\right)\mathbf{G}|_l + R^g \mathbf{P}|_l = \tau_0^g \delta_{l0} + \tau_Q^g (1 - \delta_{n1} - \delta_{n2} - \delta_{n3})\delta_{lQ} + a_l^g, \tag{21″b}$$

$$l = 0, 1, \ldots, Q, \qquad G_0 = 0, \qquad G_Q = 0\ (n > 3)$$

$$\left(\frac{2}{\Delta t} E - \nu L^u\right)\mathbf{U}|_l = \tau_0^u \delta_{l0} + \tau_Q^u (1 - \delta_{n1})\delta_{lQ} + a_l^u, \tag{21″c}$$

$$l = 0, 1, \ldots, Q, \qquad U_0 = 0, \qquad U_Q = 0\ (n > 1)$$

$$H^f \mathbf{F}|_l + H^g \mathbf{G}|_l = 0, \qquad l = \begin{cases} 0, 1, \ldots, Q, & n = 1 \\ 0, 1, \ldots, Q - 1, & n > 1, \end{cases} \tag{21″d}$$

$$\mathbf{P}_Q = 0 \qquad (n > 1).$$

Here (in contrast to Eqs. (21), (22)), $\mathbf{P} \stackrel{\text{def}}{=} (P_0, P_1, \ldots, P_Q)^T$, $P_j(\varphi) = \overset{(s)}{\tilde{p}}{}^{k+1}_{n0j} = \overset{(s)}{\tilde{p}}{}^{k+1}_{n0}|_{r=r_j}$; $\mathbf{F} \stackrel{\text{def}}{=} (F_0, F_1, \ldots, F_Q)^T$, $F_j(\varphi) = \overset{(s)}{\tilde{f}}{}^{k+1/2}_{n0j} = (\overset{(s)}{\tilde{f}}{}^{k+1}_{n0j} + \tilde{f}^k_{n0j})/2$, analogously for $\mathbf{G}$ and $\mathbf{U}$; right hand sides $a_l^{f,g,u}$ are defined by

$$a_l^f = \frac{2}{\Delta t}\tilde{f}^k_{n0l} + d^f_{n0l}\left(\frac{\overset{(s-1)}{\mathbf{q}}{}^{k+1} + \mathbf{q}^k}{2}\right), \tag{22″}$$

with similar formulas for a_l^g, a_l^u.

3. *Equations* (21) *for* $\alpha_m = n = 0$

$$\tilde{v}^{(s)k+1}_{00l} = 0, \qquad l = 0, 1, \ldots, Q, \tag{21‴a}$$

$$\left(\frac{2}{\Delta t} E - \nu L^w\right)\mathbf{W}|_l = \frac{2}{\Delta t}\tilde{w}^k_{00l} + d^g_{00l}\left(\frac{\overset{(s-1)}{\mathbf{q}}{}^{k+1} + \mathbf{q}^k}{2}\right), \tag{21‴b}$$

$$l = 1, 2, \ldots, Q, \qquad W_0 = 0$$

$$\left(\frac{2}{\Delta t}E - \nu L^u\right)\mathbf{U}|_l + \overset{(s)}{p}_x(t_{k+1}) = \frac{2}{\Delta t}\tilde{u}^k_{00l} + d^u_{00l}\left(\frac{\overset{(s-1)}{\mathbf{q}}{}^{k+1} + \mathbf{q}^k}{2}\right),$$
$$l = 1, 2, \ldots, Q, \qquad U_0 = 0, \qquad \sum_{j=0}^{Q}\gamma_j U_j = \int_0^R U^0 r\, dr. \tag{21‴c}$$

Here $\mathbf{U} \overset{\text{def}}{=} (U_0, U_1, \ldots, U_Q)^T$, $U_j = \overset{(s)}{\tilde{u}}{}^{k+1/2}_{00j} = (\overset{(s)}{\tilde{u}}{}^{k+1}_{00j} + \tilde{u}^k_{00j})/2$ and analogously for $\mathbf{W}$. Coefficients γ_j and matrices L^u, L^w are defined by

$$\gamma_j = \frac{2\varrho_j R^2}{Q}\sum_{l=0}^{Q}\varrho_l T_{2l}(r_j/R)\kappa_l, \qquad \kappa_l = \begin{cases} \frac{1}{4}\left(\frac{1}{2i+1} - \frac{1}{2i-1}\right), & l = 2i \\ 0, & l = 2i+1, \end{cases}$$
$$L^u = C + B, \qquad L^w = C + 3B.$$

4. *Relations* (24) *for* $n = 0$

$$(D + 2E)L^v\mathbf{V} + \frac{\partial}{\partial x}L^u\mathbf{U} = L^u\left((D + 2E)\mathbf{V} + \frac{\partial}{\partial x}\mathbf{U}\right), \tag{24′a}$$

$$\left((D + 2E)B - \alpha_m^2 E\right)\mathbf{P} = L^u\mathbf{P}, \tag{24′b}$$

where matrices L^v, L^u are defined by Eqs. (23′) of the previous subsection.

ACKNOWLEDGMENTS

We thank B. L. Rozhdestvensky, D. V. Chrychev, V. N. Trigub, S. G. Ponomarev, and M. I. Stoynov for valuable discussions and suggestions.

This research was supported in part by the Russian Fundamental Science Foundation Grants 93-013-17386 and 96-01-01468 and by the International Science Foundation Grant MKS-300.

REFERENCES

1. O. Reynolds, An experimental investigation of the circumstances which determine whether the motion of water shall be direct or sinuous, and of the law of resistance in parallel channels, *Philos. Trans. R. Soc. London A* **174**, 935 (1883).
2. V. G. Priymak, Results and potentialities of direct numerical simulation of turbulent viscous fluid flows in a circular pipe, *Soviet Phys. Dokl.* **36**, 28 (1991).
3. J. G. M. Eggels, F. Unger, M. H. Weiss, J. Westerweel, R. J. Adrian, R. Friedrich, and F. T. M. Nieuwstadt, Fully developed turbulent pipe flow: A comparison between direct numerical simulation and experiment, *J. Fluid Mech.* **268**, 175 (1994).
4. N. V. Nikitin, Direct numerical simulation of three-dimensional turbulent flows in circular pipes, *Izv. Acad. Nauk. Mech. Zhidk. i Gaza* **6**, 14 (1994). [In Russian]
5. P. L. O'Sullivan and K. S. Breuer, Transient growth in circular pipe flow. I. Linear disturbances, *Phys. Fluids* **6**, 3643 (1994).
6. P. L. O'Sullivan and K. S. Breuer, Transient growth in circular pipe flow. II. Non-linear development, *Phys. Fluids* **6**, 3652 (1994).
7. V. G. Priymak, Pseudospectral algorithms for Navier–Stokes simulation of turbulent flows in cylindrical geometry with coordinate singularities, *J. Comput. Phys.* **118**, 366 (1995).
8. V. G. Priymak and T. Miyazaki, Long-wave motions in turbulent shear flows, *Phys. Fluids* **6**, 3454 (1994).
9. P. G. Drazin and W. H. Reid, *Hydrodynamic Stability* (Cambridge Univ. Press, Cambridge, UK, 1981).

10. I. Herron, Observations on the role of vorticity in the stability theory of wall bounded flows, *Stud. Appl. Math.* **85**, 269 (1991).
11. L. H. Gustavsson, Direct resonance of nonaxisymmetric disturbances in pipe flow, *Stud. Appl. Math.* **80**, 95 (1989).
12. P. J. Schmid and D. S. Henningson, Optimal energy density growth in Hagen–Poiseuille flow, *J. Fluid Mech.* **277**, 197 (1994).
13. J. Gary and R. Helgason, A matrix method for ordinary differential eigenvalue problems, *J. Comput. Phys.* **2**, 169 (1970).
14. V. K. Garg and W. T. Rouleau, Linear spatial stability of pipe Poiseuille flow, *J. Fluid Mech.* **54**, 113 (1972).
15. A. Leonard and A. Wray, A new numerical method for the simulation of three-dimensional flow in a pipe, in *Proceedings, 8th Int. Conf. on Numerical Methods in Fluid Dynamics*, edited by E. Krause (Springer-Verlag, Berlin, 1982), p. 335.
16. S. A. Orszag and A. T. Patera, Secondary instability of wall-bounded shear flows, *J. Fluid Mech.* **128**, 347 (1983).
17. L. S. Tuckerman, Divergence-free velocity fields in nonperiodic geometrics, *J. Comput. Phys.* **80**, 403 (1989).
18. M. R. Khorrami, M. R. Malik, and R. L. Ash, Application of spectral collocation techniques to the stability of swirling flows, *J. Comput. Phys.* **81**, 206 (1989).
19. T. Matsushima, and P. S. Marcus, A spectral method for polar coordinates, *J. Comput. Phys.* **120**, 365 (1995).
20. S. Bouaoudia and P. S. Marcus, Fast and accurate spectral treatment of coordinate singularities, *J. Comput. Phys.* **96**, 217 (1991).
21. L. Kleiser and U. Schumann, Spectral simulation of the laminar-turbulent transition process in plane Poiseuille flow, in *Spectral Methods for Partial Differential Equations*, edited by R. G. Voigt, D. Gottlieb, and M. Y. Hussaini (SIAM-CBMS, Philadelphia, 1984), p. 141.
22. Y. L. Luke, *Mathematical Functions and Their Approximations* (Academic Press, New York, 1975).
23. C. Canuto, M. Y. Hussaini, A. Quarteroni, and T. A. Zang, *Spectral Methods in Fluid Dynamics* (Springer-Verlag, Berlin/Heidelberg, 1988).
24. P. S. Marcus, Simulation of Taylor–Couette flow. Part 1. Numerical methods and comparison with experiment, *J. Fluid Mech.* **146**, 45 (1984).
25. A. T. Patera and S. A. Orszag, Finite-amplitude stability of axisymmetric pipe flow, *J. Fluid Mech.* **112**, 467 (1981).
26. S. A. Orszag, Accurate solution of the Orr–Sommerfeld stability equation, *J. Fluid Mech.* **50**, 689 (1971).
27. B. L. Rozhdestvensky, On the applicability of finite-difference methods to the solution of the Navier–Stokes equations at large Reynolds numbers, *Dokl. Acad. Nauk SSSR* **211**, 308 (1973). [In Russian]
28. L. Shemer, I. Wygnanski, and E. Kit, Pulsating flow in a pipe, *J. Fluid Mech.* **153**, 313 (1985).
29. V. C. Patel and M. R. Head, Some observations on skin friction and velocity profiles in fully developed pipe and channel flows, *J. Fluid Mech.* **38**, 181 (1969).
30. J. Kim, P. Moin, and R. Moser, Turbulence statistics in fully developed channel flow at low Reynolds number, *J. Fluid Mech.* **177**, 133 (1987).
31. E. Laurien and L. Kleiser, Numerical simulation of boundary-layer transition and transition control, *J. Fluid Mech.* **199**, 403 (1989).
32. D. Henningson, P. Spalart, and J. Kim, Numerical simulations of turbulent spots in plane Poiseuille and boundary-layer flow, *Phys. Fluids* **30**, 2914 (1987).
33. N. D. Sandham and L. Kleiser, The late stages of transition to turbulence in channel flow, *J. Fluid Mech.* **245**, 319 (1992).
34. N. V. Nikitin, Spatial approach to the numerical simulation of turbulence in pipes, *Dokl. Acad. Nauk Rossiji* **343**, 767 (1995). [In Russian]
35. P. S. Marcus, Simulation of Taylor–Couette flow. Part 2. Numerical results for wavy-vortex flow with one travelling wave, *J. Fluid Mech.* **146**, 65 (1984).
36. P. S. Marcus and L. S. Tuckerman, Simulation of flow between concentric rotating spheres. Part 2. Transitions, *J. Fluid Mech.* **185**, 31 (1987).